ETH Zürich – EPF Lausanne

Master Thesis

Heat exchanger analysis for innovative molten salt fast reactor

---

Author:

Valerio Ariu

Supervisor:

Prof. Andreas Pautz

Prof. Horst-Michael Prasser

Dr. Konstantin Mikityuk

Dr. Carlo Fiorina

Project FAST

Laboratory for Reactor Physics and System Behavior

Paul Scherrer Institut

CH - 5232 Villigen

August 2014

To Manuela

Contents

Introduction

Background and motivation

The concept of Molten Salt Reactor (MSR) was first introduced in the frame of the Aircraft Nuclear Propulsion (ANP) program conducted by the U.S. Air Force in 1946 at the Oak Ridge National Laboratory (ORNL). The objective of the program was to evaluate the feasibility of an airplane powered through a nuclear reactor. A low power high temperature reactor (Aircraft Reactor Experiment ARE) was built to guide its development program. During the design of the ARE the possibility of dissolving the fuel into a molten salt was investigated, such that online reprocessing could be afforded. The salt heated up flowing through the core and released heat to an intermediate fluid (molten sodium) through a heat exchanger. The research reactor reached criticality in November 1954 and operated successfully for 9 days. It was shut down after all tests were performed. This first MSR demonstrated the feasibility of having a fluid acting as both fuel and coolant.

Parallel to the ANP program, research was conducted by the ORNL to apply the MSR concept to a power reactor. The Molten Salt Reactor Experiment (MSRE) was a thermal reactor designed in 1960s which operated from 1965 to 1969. Instead of using sodium as intermediate coolant, a secondary salt (eutectic mixture of LiF-BeF$_2$) was used. A shell and tube heat exchanger (STHE) transferred heat from primary to intermediate salt, the heat was then dissipated to the atmosphere through a radiator. The power generated by the reactor was 7.4 MW$_{th}$, with a primary salt outlet temperature of 936 K. Despite the successful achievements of the experiment, the U.S. Atomic Energy Commission (AEC) shut down the MSRE program in 1973 and focussed the investments to sodium cooled fast reactors.

The Generation IV International Forum (GIF IV) selected in 2001 the MSR as one of six innovative concepts for the new generation of nuclear reactors [53]. The MSR was studied in the frame of the EVOL project (Evaluation and Viability Of Liquid fuel fast reactor system) and developed into a thorium based Molten Salt Fast Reactor (MSFR) [3]. In

open literature studies on the MSFR focus mainly on fuel cycle analysis, neutronics and core thermal hydraulics [4]. These analysis determined among other parameters the primary salt composition, flow rates, residence time (in-core and out-of-core) and temperatures in the hot and cold legs. Some of the main features of single components of the primary circuit as pumps, reprocessing unit and heat exchangers are drafted in [3, 7, 8], but a specific design of these was not yet proposed for the MSFR. An extensive study on the thermal hydraulics of the complete primary circuit could not be found in literature. Moreover models of the intermediate circuit and power conversion system directly related to the MSFR were not proposed.

Objectives and outline of the work

The first objective of this work is an assessment of possible solutions for the primary heat exchanger (HX) of the MSFR (Chapter 1), since no specific studies were found in open literature. Different types of heat exchanger are considered in the frame of the characteristics of the MSFR [4]. A heat exchanger between two molten salts for nuclear application was realized for the MSRE, and was investigated during a preparatory semester work [16]. By virtue of the positive experience obtained during its operation, the possibility of using the same type of heat exchanger (shell and tube) for the MSFR is here examined. Beside the experience in heat transfer with molten salts from the MSRE, in the recent past the interest on molten salts has been growing for applications in solar energy generation and storage, in particular for Concentrated Solar Power plants (CSP) [31, 32]. Studies on CSP are therefore valuable assets for a preliminary assessment of the primary heat exchanger. Based on the characteristics and the technological limits of currently available heat exchangers, a preliminary selection for the primary HX for the MSFR is conducted. In addition to the shell and tube heat exchanger, a second type of heat exchanger (printed circuit) is selected for a thorough analysis.

A model is developed for the preliminary design of the selected types of heat exchanger. The geometry of the heat exchanger, the characteristics of the flows (as flow rates, flow regime and pressure drop) and the heat transfer between the fluids are modeled following the constraints of the MSFR regarding power, inlet and outlet temperature of the primary salt, pressure drops and salt volume. A preliminary design, following guidelines for manufacturing heat exchangers in industry, is then obtained for the primary heat exchanger of the MSFR. The intermediate salt to be used for the MSFR is not yet defined. Two different intermediate salts are considered in this thesis work (FliBe and FliNaK). Based on their thermophysical characteristics different geometrical designs are obtained through the developed model for the primary heat exchanger.

After the selection and the design of a heat exchanger of the MSFR, its performance is investigated in steady state and accidental conditions through simulation with thermal hydraulic code TRACE (Chapter 2). A simplified model for the closed primary circuit of the MSFR is implemented in TRACE with a pipe representing the core, the heat exchanger, the pump and the respective piping. The intermediate circuit is modeled through a closed circuit, with the balance of plant modeled through an intermediate heat exchanger. A simultaneous pump trip in the primary and intermediate circuit – representing a station black out accident (SBO) – is simulated. The behavior of the MSFR using the proposed heat exchanger is investigated in accidental conditions and the temperature evolution in the primary and intermediate circuit are analyzed. Different height differences between the heat source and heat sink of the primary circuit (core – primary HX) and of the intermediate circuit (primary HX – intermediate HX) are tested. The impact on the natural circulation of the salts, therefore on the safety of the MSFR, is examined. Preliminary guidelines are proposed for the design of the primary and intermediate piping system concerning the safety of the MSFR in case of a SBO accident.

Chapter 1

Choice and preliminary design of the heat exchangers of the Molten Salt Fast Reactor

1.1   Introduction

The objective of this chapter is to present possible solutions and propose a preliminary design for the primary heat exchanger (HX) for the Molten Salt Fast Reactor (MSFR). A preliminary assessment of the state-of-the-art technology and currently available materials is conducted. The options among different types of heat exchangers are evaluated meeting the constraints of the MSFR, in particular as far as temperatures, pressures and salt volumes are concerned. This preliminary selection limits the options to two types of heat exchangers, based on present technological, material- and construction-related limits. As a next step, the two types of heat exchanger are investigated in depth. A software tool *ad hoc* developed for their preliminary design is presented. The resulting preliminary design of the primary heat exchanger is discussed. Several working fluids for the power cycle are presented and their characteristics are discussed. Finally a design for the intermediate heat exchanger of the MSFR is proposed.

1.2   Preliminary selection of possible candidates for the MSFR heat exchanger

The primary heat exchanger is the component responsible for the heat transfer from the primary salt to the intermediate salt. In order to perform an assessment on possible

heat exchangers, the basic characteristics of the salts and the flow in the primary circuit must be briefly described. A description of the MSFR design and characteristics is given further on in Section 1.4.1.

The MSFR was studied and designed in the frame of the EVOL project (Evaluation and Viability Of Liquid fuel fast reactor systems). The studies fixed the choice of the primary salt, the core inlet and outlet temperatures as well as the in-core and out-of-core residence time of the salt. This limits the salt inventory in the heat exchanger.

The primary heat exchanger is the main actor of this study, therefore the temperatures are referred to it. The primary salt inlet temperature $T_{F,\text{in}}$ corresponds to the core outlet temperature, which is fixed at 1023 K by design of the MSFR. The outlet temperature of the primary salt $T_{F,\text{out}}$ is constraint to 923 K. The inlet temperature for the intermediate salt $T_{C,\text{in}}$ is to be defined, as well as the temperature drop between the primary and the intermediate salt (which will influence the power cycle, discussed further on in Section 1.5.1). The two salts are expected to flow at pressures slightly above atmospherical pressure, without significant differences in pressure between them. No pressurization is needed from a thermodynamical point of view. Low pressure losses are wished, such that energy requirement for the pumping systems are minimized.

Without entering technical details of the designed reactor, several design criteria are set for the preliminary choice of the primary heat exchanger:

- Material resistance to high temperatures, up to 750°C

- Low pressure drops allowed

- Low salt inventory

In the following paragraphs several types of heat exchanger are described and compared, with respect to the constraints of the MSFR. At the end of the section a preliminary choice is performed.

The shell and tube heat exchanger (STHE) is the most commonly used HX and represents the "workhorse" of industrial process heat transfer. It has many applications in the power generation, petroleum refinery, chemical industries and process industries. It is used as oil cooler, condenser, feed water heater, etc.[37]

The Tubular Exchanger Manufacturers' Association (TEMA) propose standards for the design of STHE, which are followed in most countries [1]. The description given in this work is consistent in correlation and nomenclature with TEMA standards, unless

specified. A schematic representation of a STHE can be seen in Fig. 1.1. In the following a description of the main components is given.
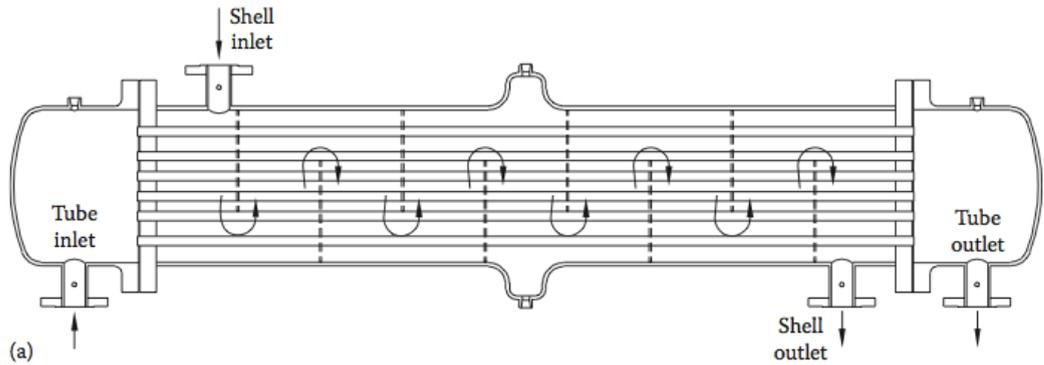
FIGURE 1.1. Schematic representation of a STHE [1]

A STHE consists of a bundle of tubes contained in a cylindrical shell. The heat transfer mechanism between the fluids is conduction across tube walls, with one fluid flowing in the tubes and one fluid in the shell. The tubes are arranged in a bundle with different possible layouts: square, rotated square, triangular and rotated triangular (shown in Fig. 1.2). The rotated layouts are not widely used, but are presented here for completeness. Different arrangements for the tube bundle inside the shell are possible: single pass tube bundle, two pass (U-Tube), four pass, six pass, ... up to sixteen passes, depending on the necessary characteristics. The most common tube arrangement is U-Tube. This configuration is easy to manufacture and allows the possibility for the tube thermal expansion in longitudinal direction, compared to a single pass tube arrangement.
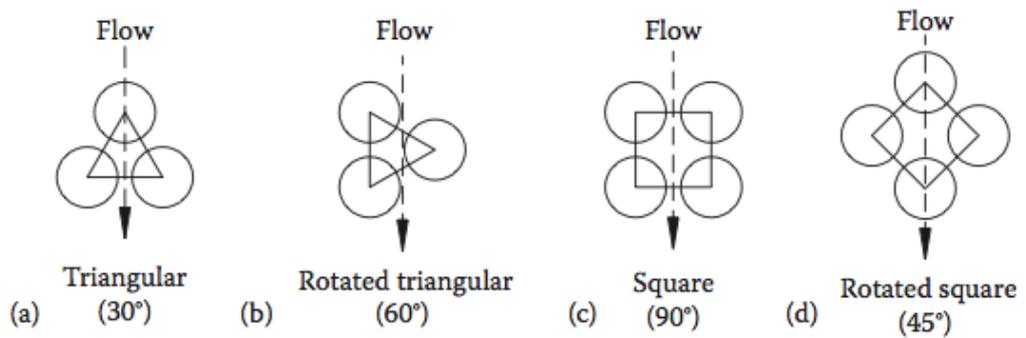
FIGURE 1.2. Four possible tube arrangements in a STHE [37]

Several shell types can be chosen for the design of a STHE and are defined by TEMA, see Fig. 1.3. Type E shell ("One pass shell") is the most commonly used.

Baffles are support plates for the tubes inside the shell. The purpose of baffles is on one hand to maintain the spacing between the tubes during operation and on the other hand
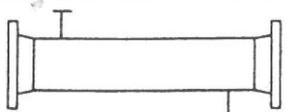
	SHELL TYPES
E	ONE PASS SHELL
F	TWO PASS SHELL WITH LONGITUDINAL BAFFLE
G	SPLIT FLOW
H	DOUBLE SPLIT FLOW
J	DIVIDED FLOW
K	KETTLE TYPE REBOILER
X	CROSS FLOW
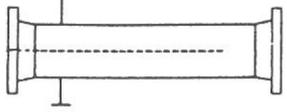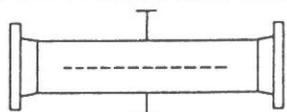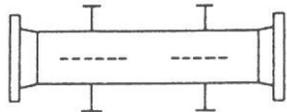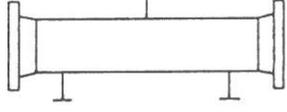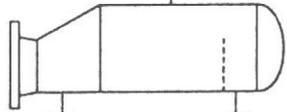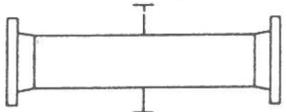
FIGURE 1.3. Standard TEMA nomenclature for STHE components [1]

to change the flow pattern of the shellside fluid. Depending on the required application, the number, the height and the spacing between the baffles can be chosen in order to modify the heat transfer properties (by allowing crossflow over the tubes) and/or modify the pressure drop across the shell.

This type of heat exchanger was used during the Molten Salt Reactor Experiment (MSRE) conducted by the Oak Ridge National Laboratory (ORNL) in the 1960s. Furthermore, it was designed to be used for the Molten Salt Breeder Reactor (MSBR), which was an innovative project of ORNL. The breeder reactor was designed, but the program was canceled before construction in 1976 due to budget constraints [15, 12].

The main advantages and disadvantages of a **STHE** for a salt-salt heat exchanger are here summarized:

+ Manufacturing experience

+ Wide range of working pressures

+ Wide choice of materials (important for corrosion and erosion of the salts)

+ Possibility to enhance the heat transfer by changing the geometry (tube diameter, fins, baffles, etc.)

– Low heat transfer surface area density

– Expensive per unit of heat transfer area

– Low heat transfer efficiency

Plate heat exchangers   (PHE) are used for liquid-liquid duties, including heating and ventilating, food processing, pharmaceuticals and fine chemicals, petroleum and chemical industries, power generation, offshore oil and gas production, etc. [37] This type of heat exchanger is replacing tubular heat exchangers in many application fields.

A PHE consists of a number of metal plates provided with gaskets, where each fluid passes through alternate channels. Pure counterflow can be achieved. This reduces the temperature drop between the two fluids and increases the efficiency of the heat exchanger. The flow regime of high viscous fluid can be made turbulent through the geometrical arrangement of the channels. A turbulent flow regime decreases the thermal resistivity of the fluid, improving the heat transfer. An example of PHE is shown in Fig. (1.4) A description of the main components is given in the following.
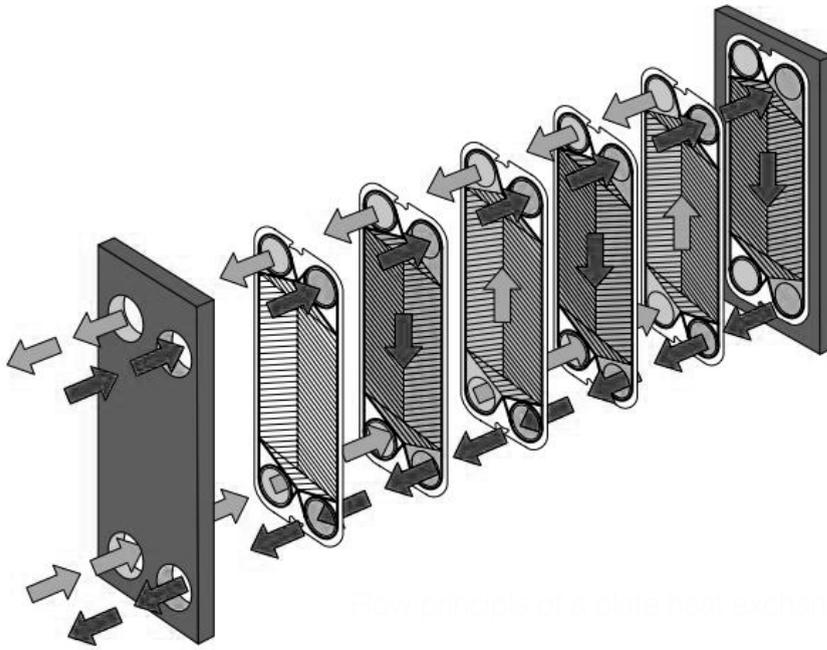
FIGURE 1.4. Flow schematic view of a plate heat exchanger [48]

The plates can be corrugated and embossed to increase turbulence and surface area, therefore the overall heat transfer coefficient. The plate thickness can be reduced down to 0.6 mm, in order to minimize the heat loss through the metal.

The gaskets are composed of different materials and should be chosen based on temperature, pressure, and chemical compatibility with the fluids. In order to increase the temperature and pressure limits, the gaskets can be avoided by using fully welded plates ("All-welded plate exchanger" type). Due to the high temperature constraints of the MSFR, gaskets must be avoided. The main drawback of "All-welded plate exchanger" is the impossibility to perform maintenance and mechanical cleaning.

Other options for PHE are described in detail in [37].

The main advantages and disadvantages of **PHE** for a salt-salt system are here summarized:

+ High turbulence and true counterflow lead to an efficient heat transfer

+ Low hold-up volume (low salt inventory)

+ Wide choice of materials (important for corrosion and erosion of the salts)

+ Small temperature drop

+ Less erosion-corrosion issues compared to STHE

 – No mechanical cleaning possible

 – High flow rates in small channels involve high pressure drops

Compact heat exchangers   (CHE) are the response to the need of space-saving, light-weight and economical heat exchangers. The main characteristic is the high surface area density: a large heat transfer area over a small volume. CHE comprehend Tube-fin, Plate-fin heat exchangers and Regenerators. The latest are used for gas-gas applications and are not described further on.

Tube-fin HX (shown in Fig. 1.5) are suitable when a high pressure difference and/or a significant difference in the heat transfer coefficient between the fluids occurs. This type of HX is widely used for condensers and evaporators. No applications for heating were found, therefore TFHE are discarded for the use in MSFR.
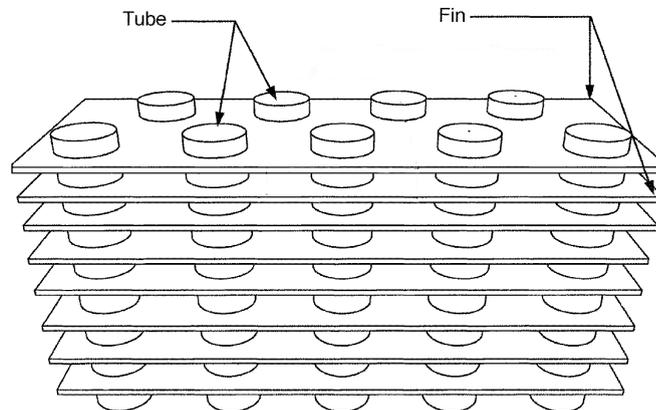
FIGURE 1.5. Tube-fin heat exchanger [49]

Plate-fin HX (PFHE) (shown in Fig. 1.6) are used for heat exchanger between gases, liquids or both, for condensation and boiling. PFHE consist of a stack of alternate flat plates and fin corrugations [37], where the flow arrangement can be crossflow or counterflow. PFHE offers large heat transfer area density, compared to the area density of a STHE. This type of heat exchanger operates at low pressures. A wide selection of materials (e.g. stainless steels and heat-resistant alloys) for PFHE allows the employment of high temperature fluids.

The main advantages and disadvantages of **PFHE** for a salt-salt system are here summarized:

 + Large heat transfer area density

 + High maximum operating temperature (800°C)

 + High effectiveness (in the order of 95%)
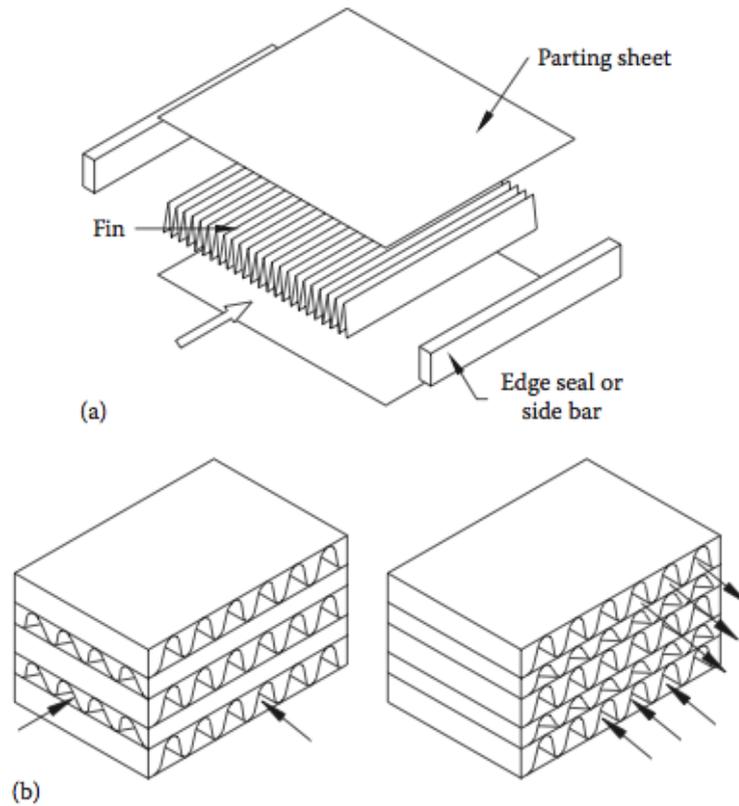
FIGURE 1.6. Plate-fin heat exchangers: (a) basic elements, (b) two types of flow arrangements [37]

+ Small pressure drops

− Flow maldistribution causes a non-uniform heat exchanger performance, for a large front area

− Complex startup and controls with respect to STHE

Printed circuit heat exchanger (PCHE) is a relatively new type of heat exchanger manufactured by Heatric™. PCHE have been a well-established technology in the hydrocarbon processing, petrochemical and refining industries. This type of HX is similar by design to the PFHE (as can be seen in Fig. 1.7), it is compact, highly effective and has a large surface area density. The difference between PCHE and PFHE is the technique used to manufacture the HX. The PCHE are manufactured with a technique called "diffusion bonding": high pressures and high temperatures are applied to the layers and atoms intermingle through diffusion over time until the plates are welded. No joints nor welds results from this manufacturing process, therefore weaknesses are reduced [40].

The flow channels can be parallel (counterflow) or perpendicular (crossflow).
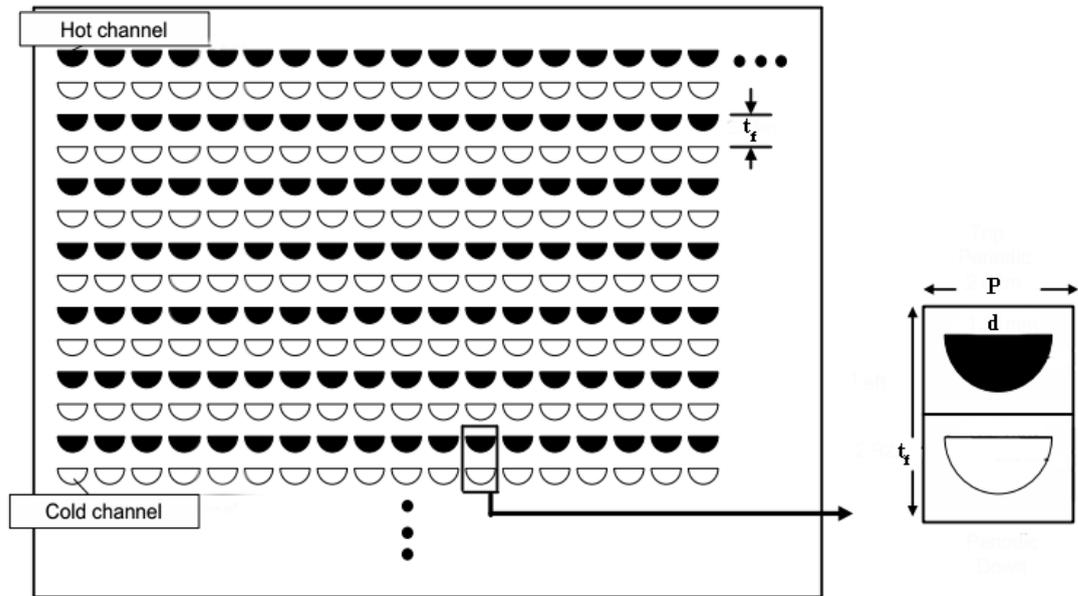
FIGURE 1.7. Cross sectional scheme of a PCHE [43]

The main advantages and disadvantages of **PCHE** for a salt-salt system are here summarized:

- + High heat transfer area density (up to 2500 m^2/m^3)

- + High maximum operating temperature (900°C)

- + High effectiveness (in the order of 98%)

- + Small pressure drops

- + Light and compact

- – New technology

- – Ongoing development of materials

The primary selection for the MSFR primary heat exchanger is performed by considering the criteria described at the beginning of the section. The experience with the *shell and tube heat exchanger* during the MSRE and its consideration for the MSBR make this type of HX a strong candidate for the MSFR. Besides this, it is considered the reference among heat exchangers. As a second candidate the *printed circuit heat exchanger* is chosen, based on the high degree of compactness, the expectation of low pressure drops and the simplicity of the concept.

Further on a basic method for the design of the two candidate heat exchangers is presented.

1.3 Tool development for the basic design of a heat exchanger

In the present section a software tool is described for a preliminary design of the two types of heat exchanger: STHE and PCHE.

The starting point of this analysis are the constraints of the MSFR on power, primary salt temperatures and salt properties. The results obtained from the tool will be the overall heat transfer coefficient, the pressure drop for each fluid, the salt inventory in the heat exchanger, the velocities of the salts and the dimensions of the heat exchanger.

1.3.1 Shell and tube heat exchanger – Tool for design

The design of a shell and tube heat exchanger is usually provided by a dedicated software. This types of software take into account, besides heat transfer properties and flow properties, also economical aspects. Since such an exhaustive analysis is not required for this thesis, a simpler approach is proposed to design a shell and tube heat exchanger.

The heat transfer coefficient U (W/m^2·K) of a heat exchanger is often coupled to the heat transfer area A (m^2), forming the overall heat transfer coefficient UA expressed in W/K.

The required overall heat transfer coefficient $(UA)_{\text{req}}$ for a given task can be determined knowing the power to be exchanged $\dot{Q}$ and the mean temperature difference ΔT_M between the fluids:

$$\dot{Q} = (UA)_{\text{req}}\Delta T_M, \tag{1.1}$$

therefore

$$(UA)_{\text{req}} = \frac{\dot{Q}}{\Delta T_M}, \tag{1.2}$$

For a pure counterflow heat exchanger, where the two fluids flow in opposite directions, the mean temperature difference is given by the logarithmic mean temperature difference (subscript h refers to the hot fluid to be cooled, c to the cold fluid to be heated):

$$\Delta T_M = \Delta T_{\text{LM}} = \frac{(T_{h,\text{in}} - T_{c,\text{out}}) - (T_{h,\text{out}} - T_{c,\text{in}})}{\ln(\frac{T_{h,\text{in}}-T_{c,\text{out}}}{T_{h,\text{out}}-T_{c,\text{in}}})}. \tag{1.3}$$

For a shell and tube heat exchanger the logarithmic mean temperature difference has to be corrected for crossflow. This correction factor applies only in case where the tubes are arranged into the shell with an even number of passes. The logarithmic mean temperature has to be multiplied by a factor F (also called the F-factor), depending on the temperature ratios R and P:

$$R = \frac{\Gamma_c c_{p,c}}{\Gamma_h c_{p,h}} = \frac{T_{h,\text{in}} - T_{h,\text{out}}}{T_{c,\text{out}} - T_{c,\text{in}}},$$

$$P = \frac{T_{c,\text{out}} - T_{h,\text{in}}}{T_{h,\text{in}} - T_{c,\text{in}}},$$

where Γ_i is the mass flow and $c_{p,i}$ is the heat capacity. The F-factor can be then interpolated from Fig. 1.8, in case where the hot fluid is placed in the shellside, as it is often the case for shell and tube heat exchanger.
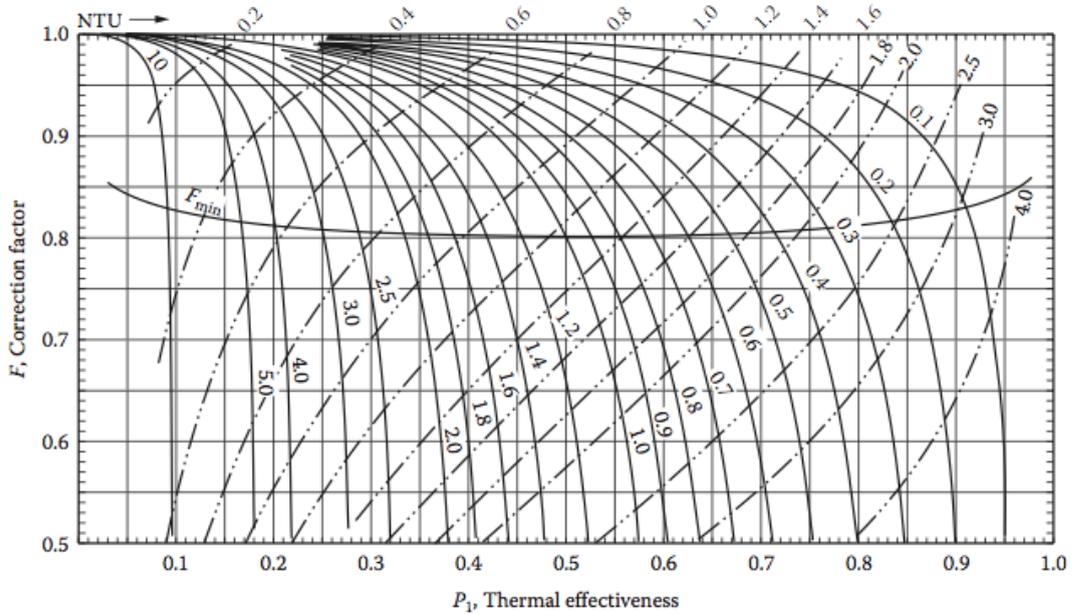
FIGURE 1.8. F-Factor as function of R and P for a E-type shell [37]

Finally the mean temperature can be determined:

$$\Delta T_M = F \Delta T_{\text{LM}}.$$

The design process of a STHE is iterative. The heat transfer coefficient needs to be initially estimated (U_{est}) to begin the iterations (see Section 1.4.2). For commonly used fluids (e.g. water, oil, gases, etc.) typical heat transfer coefficients are tabulated [1]. This initial guess is needed to estimate the total heat transfer area to exchange the heat: $A = (UA)_{\text{req}}/U_{\text{est}}$.

The heat exchanger is designed following TEMA standards. In principle some geometrical parameters could be varied, but it was decided to maintain the proposed TEMA correlations. The required result is not the optimal design of the heat exchanger but a preliminary design to be compared with other possible solutions, therefore a fine tuning of each parameter is not necessary. TEMA correlations are:

- $L_{tp} = 1.25d_o$, the tube pitch is determined by the outer diameter of the tube

- $L_{bc} = 0.3D_s$, the baffle spacing is determined by the shell diameter

- $L_{sb} = (3.1 + 0.004D_s)/1000$, the shell-to-baffle diametral clearance is determined by the shell diameter

- $L_{bb} = (12 + 5D_s)/1000$, the bundle-to-shell diametral clearance is determined by the shell diameter

- $L_{tb} = 0.0008$ m, the tube-to-baffle diametral clearance is fixed

- $L_b = 0.005$ m, the tube sheet thickness is fixed

- $SS = 0.2$, the number of sealing strips per crossflow row

- $B_c = 25\%$, the baffle-cut as percent of the shell diameter

The heat exchanger main design parameters are described graphically in Figs. 1.9, 1.10 and 1.11.
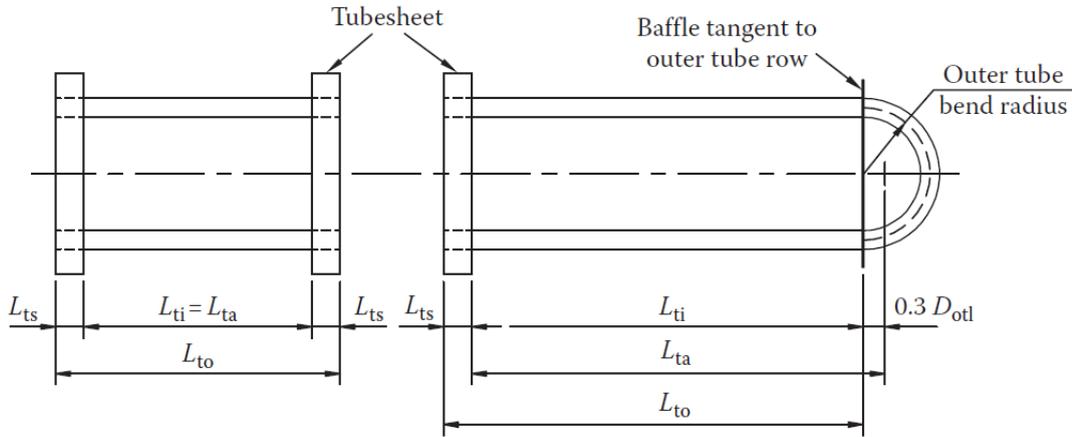
FIGURE 1.9. Schematic representation of a U-Tube [37]

The following parameters need to be determined: d_o the tube outer diameter, t_w the tube thickness, L_{tube} the tube length, the tube layout, N_t the number of tubes, N_p the number of tube passes and D_s the shell diameter.
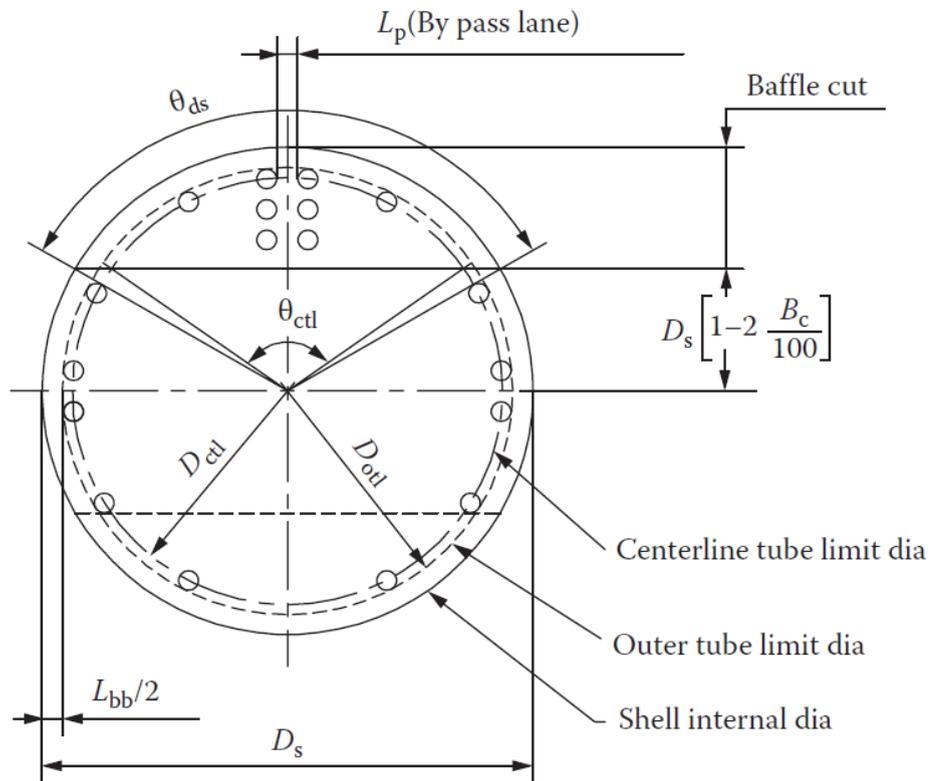
FIGURE 1.10. Cross sectional view of the shell of the heat exchanger [37]
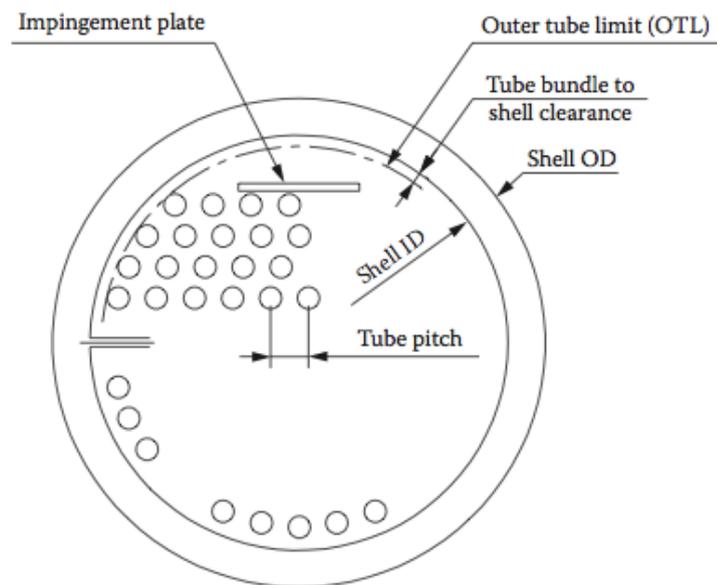
FIGURE 1.11. Additional description of the shell cross sectional parameters [37]

The velocity on the tubeside has to be chosen by the user. The maximal velocity for the salts is fixed to 5 m/s to avoid excessive erosion [3].

The velocity in the tubes is given by

$$v_{\text{tube}} = \frac{\dot{V}}{\pi \frac{d_i^2}{4}} \frac{N_p}{N_t}, \tag{1.4}$$

where $\dot{V}$ is the volumetric flow rate (further on called flow rate), obtained from $\dot{V} = \frac{\Gamma}{\rho}$, where ρ is the tubeside fluid density. The ratio between the number of tube passes and number of tubes $\frac{N_p}{N_t}$ can be determined from Eq. 1.4 after setting the velocity in the tubes. The number of tubes N_t is defined as the total number of tubes in a cross sectional view of the heat exchanger. To count only the tubes connected to the inlet nozzle, the total number of tubes must be divided by the number of tube passes N_p. Usually an even number of passes is chosen (2, 4 or 6). Determining the number of passes will determine the number of tubes N_t.

The length of the tubes L_{tube} per tube pass (also called "active shell length") is determined using the tube outer diameter d_o, the required total area A_{req} and the number of tubes N_t (determined in the previous step):

$$L_{\text{tube}} = \frac{A_{\text{req}}}{\pi d_o N_t}.$$

It is important to notice that the heat transfer area is considered as the tube area, calculated using the *outer diameter* of the tubes. The use of the averaged diameter $(d_o + d_i)/2$ can be found in literature. A correction factor for the area is applied further on for the calculation the heat transfer coefficient U.

The centerline tube limit D_{ctl}, described in Fig. 1.10, can be estimated with the help of the number of tubes N_t, the tube pitch L_{tp} and the tube layout (triangular, square or rotate square)[33]:

$$D_{ctl} = \sqrt{N_t C_1 L_{tp}^2/0.78},$$

where C_1 is the tube layout constant, $C_1 = 0.86$ for $30°$ arrangement, $C_1 = 1$ for $45°$ and $90°$ arrangement (see Fig. 1.2).

The shell diameter D_s can be determined from

$$\begin{aligned} D_s &= D_{ctl} + d_o - L_{bb} \\ &= D_{ctl} + d_o - (12 + 5D_s)/1000, \end{aligned}$$

therefore

$$D_s = 0.995 \left(D_{ctl} + \frac{12}{1000} + d_o \right),$$

and

$$D_{\text{otl}} = D_s - L_{\text{bb}} = 0.995 D_s - 12/1000.$$

The number of baffles N is necessary for the design and for the calculation of the pressure drop in the shellside; it can be expressed as

$$N = \frac{L_{\text{tube}}}{(L_{bc} + t_b)} - 1.$$

The volumes of the salts in the shell and in the tubes can be also determined

$$V_{\text{tube}} = \frac{d_i^2 \pi}{4} N_t L_{\text{tube}}$$

$$V_{\text{shell outer}} = \left(D_s^2 - (D_{ctl} + d)^2 \right) \frac{\pi}{4} L_{\text{tube}}$$

$$V_{\text{shell inner}} = \left(D_{otl}^2 - d_o^2 N_t \right) \frac{\pi}{4} L_{\text{tube}}$$

$$V_{\text{shell}} = V_{\text{shell outer}} + V_{\text{shell inner}}.$$

The volume of salt in the shell is divided in two parts: an inner region with tubes, and an outer region between the shell and the tube bundle.

Table 1.1 summarizes the parameters needed for the design of the STHE. "Parameter*" indicates the values determined by the constraints of the problem, i.e. by the reactor design.

1.3.1.1   HTC determination for the wall interface of a STHE

The heat transfer coefficient for the shell and tube heat exchanger is determined by three components : the shellside, the tubeside and the wall interface heat transfer coefficient,

$$U = \left(\frac{1}{U_{\text{shellside}}} + \frac{d_o}{d_i} \frac{1}{U_{\text{tubeside}}} + \frac{d_o \ln \frac{d_o}{d_i}}{2} \frac{1}{U_{\text{wall}}} \right)^{-1} \tag{1.5}$$

where d_o and d_i are the outer and inner diameter of the tubes. As described previously, the area defined in Eq. 1.1 as A_{req} is determined by the outer surface of the tubes.

TABLE 1.1. Parameters for the design of the shell and tube heat exchanger

$\dot{Q}$	Parameter*
$T_{h,\text{in}}$	Parameter*
$T_{h,\text{out}}$	Parameter*
$T_{c,\text{in}}$	Parameter
$T_{c,\text{out}}$	Parameter
U_{est}	Estimated
Tube layout	Parameter
d_o	Parameter
t_w	Parameter
N_p	Parameter
v_{tube}	Constraint
L_{tube}	Determined
N_t	Determined
D_s	Determined
D_{otl}	Determined
D_{ctl}	Determined
L_{tp}	Determined by TEMA
L_{bc}	Determined by TEMA
L_{sb}	Determined by TEMA
L_{bb}	Determined by TEMA
L_{tb}	Fixed by TEMA
L_b	Fixed by TEMA
SS	Fixed by TEMA
B_c	Fixed by TEMA

In order to weight the three components of the heat transfer coefficient of Eq. 1.5 two geometrical correction factors relative to the outer and inner diameter are introduced.

The **heat transfer coefficient for the wall interface** depends on the tube thickness t_w and on the thermal conductivity k_w of the material

$$U_{\text{wall}} = \frac{k_w}{t_w}.$$

1.3.1.2   HTC and Δp determination for the shellside of the STHE

The **heat transfer coefficient for the shellside** can be determined using two different methods: the Bell-Delaware method and the Wills and Johnston method. The first one is more widely recognized as a standard for the design of the heat exchangers, while the

second should be preferred in the light of its more fundamental nature [1]. Both methods are presented here.

The Bell-Delaware method   was developed to estimate the heat transfer coefficient in the shellside. It estimates first the ideal heat transfer coefficient assuming complete crossflow between the fluid in the shellside and tube bundle. As a second step, correction factors for the following elements are introduced [1]:

- Effect of the baffle configuration (i.e. a recognition of the fact that only a fraction of the tubes are in pure cross-flow) (J_C)

- Leakage through the gaps between the tubes and the baffles and the baffles and the shell, respectively (J_L)

- Bypass of the flow around the gap between the tube bundle and the shell (J_B)

In the following, all fluid properties are referred to the shellside fluid, unless specified.

The ideal shellside heat transfer coefficient   The calculation of the ideal shellside heat transfer coefficient is based on the assumption of complete crossflow between the shellside fluid and the tube bank.

The maximal velocity near the centerline is determined by

$$v_{\max} = \frac{\dot{V}}{S_m} \tag{1.6}$$

where S_m is the minimal crossflow area at bundle centerline:

$$S_m = L_{bc} \left(D_s - D_{otl} + \frac{D_{otl} - d_o}{L_{tp}} \left(L_{tp} - d_o \right) \right). \tag{1.7}$$

For tube layouts differing from square or triangular, a different correlation for the crossflow area can be found in [1].

The Reynolds number and the Prandtl number are determined by

$$\mathrm{Re} = \frac{\rho v_{\max} d_o}{\mu}$$
$$\mathrm{Pr} = \frac{c_p \mu}{k}$$

where ρ is the density, μ is the viscosity, c_p the heat capacity and k the thermal conductivity of the shellside fluid.

The ideal shellside heat transfer coefficient is computed using correlations which have a standard deviation of about 25% for laminar flow and 15% for turbulent flow [1]. The correlation for the Nusselt number is given by

$$\mathrm{Nu} = a\ \mathrm{Re}^m\ \mathrm{Pr}^{0.34}F_1,$$

therefore the ideal shellside coefficient

$$U_{\text{shellside, ideal}} = \frac{\mathrm{Nu}\ k}{d_o},$$

where the constants a and m are listed in Table 1.2. Factor F_1 corrects for the variation in physical properties between the surface and the bulk: $F_1 = \left(\frac{\mathrm{Pr_B}}{\mathrm{Pr_W}}\right)^{0.26}$.

TABLE 1.2. a and m parameters as function of Reynolds number and tube layout

Tube layout	a	m	Reynolds
in line banks	0.742	0.431	$\mathrm{Re} < 300$
	0.211	0.651	$300 < \mathrm{Re} < 2 \cdot 10^5$
	0.116	0.7	$2 \cdot 10^5 < \mathrm{Re} < 2 \cdot 10^6$
staggered banks	1.309	0.36	$\mathrm{Re} < 300$
	0.273	0.635	$300 < \mathrm{Re} < 2 \cdot 10^5$
	0.124	0.7	$2 \cdot 10^5 < \mathrm{Re} < 2 \cdot 10^6$

Calculation of the correction factors J_i

- The configuration correction factor:

  For sake of simplicity the baffle length is expressed by $L_c = B_c D_s$

  The fraction of tubes in crossflow is

  $$F_c = \frac{1}{\pi}\left(\pi + \frac{2\left(D_s - 2L_c\right)}{D_{otl}}\sin\left(\cos^{-1}\frac{D_s - 2L_c}{D_{otl}}\right)2 - \cos^{-1}\left(\frac{D_s - 2L_c}{D_{otl}}\right)\right).$$

  The configuration correction factor is given by

  $$J_C = 0.55 + 0.72F_c.$$

- The leakage correction factor

$$S_{sb} = \frac{D_s L_{sb}}{2} \left(\pi - \cos^{-1} \left(1 - \frac{2L_c}{D_s} \right) \right) \qquad \text{shell-to-baffle leakage area}$$

$$S_{tb} = \frac{\pi d_o L_{tb}}{2} N_t \frac{1 + F_c}{2} \qquad \text{tube-to-baffle leakage area}$$

$$r_{lm} = \frac{S_{sb} + S_{tb}}{S_m}$$

$$r_s = \frac{S_{sb}}{S_{sb} + S_{tb}}$$

$$x = -0.15(1 + r_s) + 0.8$$

The leakage correction factor is given by:

$$J_L = \frac{0.44}{1 - r_s} + [1 - 0.44(1 - r_s)] \exp\left(-2.2 r_{lm}\right)$$

The correlation used for J_L was found in [33]. J_L can also be interpolated using r_{lm} and r_s from Fig. 1.12.
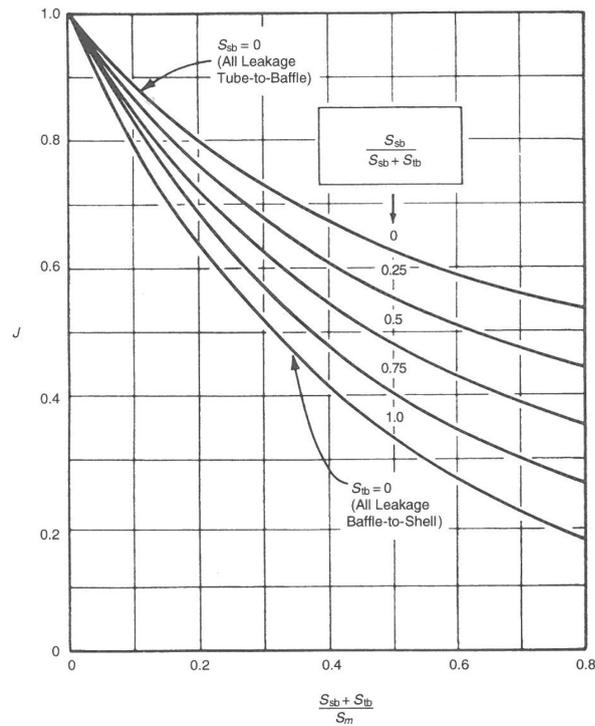
FIGURE 1.12. Correction factor for the effect of tube-to-baffle and baffle-to-shell leakage for calculating heat transfer coefficients [1]

- Bypass correction factor

$$F_{bp} = \frac{(D_s - D_{otl}) L_{bc}}{S_m} \qquad \text{bypass area fraction}$$

The number of crossflow rows N_c depends on the tube layout:

$$\begin{cases} N_c = D_s \dfrac{(1 - 2L_c/D_s)}{L_{tp}} & \text{for square layout} \\[3mm] N_c = D_s \dfrac{(1 - 2L_c/D_s)}{0.866 L_{tp}} & \text{for triangular layout} \end{cases} \tag{1.8}$$

The number of sealing strips is given by

$$N_{ss} = \lceil N_c SS \rceil. \tag{1.9}$$

The bypass correction factor is given by

$$\begin{cases} J_B = 1 & \text{for } SS > 0.5 \\[2mm] J_B = \exp\left(-1.35 F_{bp} \left(1 - (2r_{ss})\right)^{1/3}\right) & \text{else} \end{cases}$$

or can be extrapolated from Fig. 1.13

Finally the **shellside heat transfer coefficient** is given by:

$$U_{\text{shellside}} = U_{\text{shellside, ideal}} J_C J_L J_B. \tag{1.10}$$

Pressure drop calculation   The method to calculate the pressure drop with the Bell-Delaware method is similar to the procedure to calculate the heat transfer coefficient. First the ideal pressure drop for complete crossflow is calculated, as a second step correction factors are applied.

The ideal crossflow pressure drop for the shellside fluid, neglecting inlet and outlet nozzles, is given by

$$\Delta p_c = N_c K_f \left(\frac{1}{2} \rho v_{\text{max}}^2\right) \tag{1.11}$$

where K_f is a factor which depends on the Reynolds number and on the layout (for fixed pitch-to-diameter ratio $L_{tp}/d_o = 1.25$):

For square tube banks

$$\begin{cases} K_f = 0.272 + \dfrac{0.207 \cdot 10^3}{\text{Re}} + \dfrac{0.102 \cdot 10^3}{\text{Re}^2} - \dfrac{0.286 \cdot 10^3}{\text{Re}^3} & \text{Re} < 2300 \\[4mm] K_f = 0.267 + \dfrac{0.249 \cdot 10^4}{\text{Re}} - \dfrac{0.927 \cdot 10^7}{\text{Re}^2} + \dfrac{10^{10}}{\text{Re}^3} & 2300 < \text{Re} < 2 \cdot 10^6 \end{cases}$$
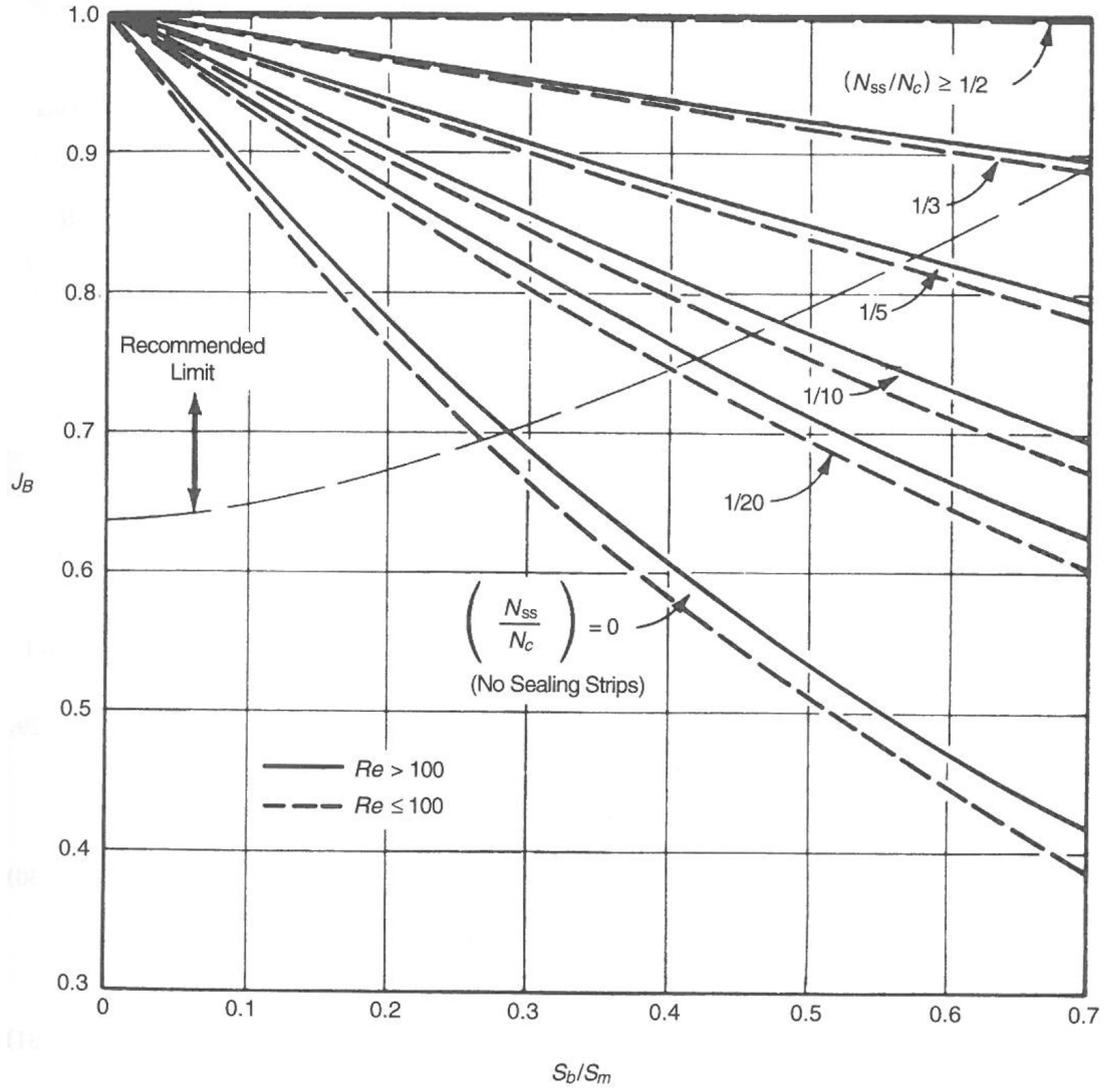
FIGURE 1.13. Correction factor for the effect of bypass on the heat transfer coefficient. N_{ss} is the number of pairs of sealing strips and N_c is the number of cross flow rows. [1]

For triangular tube banks

$$\begin{cases} K_f = 0.795 + \dfrac{0.247 \cdot 10^3}{\text{Re}} + \dfrac{0.335 \cdot 10^4}{\text{Re}^2} - \dfrac{0.155 \cdot 10^4}{\text{Re}^3} + \dfrac{0.241 \cdot 10^4}{\text{Re}^4} & \text{Re} < 2300 \\[3mm] K_f = 0.245 + \dfrac{0.339 \cdot 10^4}{\text{Re}} - \dfrac{0.984 \cdot 10^7}{\text{Re}^2} + \dfrac{0.133 \cdot 10^{11}}{\text{Re}^3} - \dfrac{0.599 \cdot 10^{13}}{\text{Re}^4} & 2300 < \text{Re} < 2 \cdot 10^6 \end{cases}$$

The number of effective crossflow rows in the window zone N_{cw} and the window flow area S_w are given by

$$N_{cw} = \frac{0.8 L_c}{L_{tp}}$$

$$S_w = \frac{D_s^2}{4}\left(\cos^{-1}\left(1 - 2\frac{L_c}{D_s}\right) - \left(1 - 2\frac{L_c}{D_s}\right)\sqrt{1 - \left(1 - 2\frac{L_c}{D_s}\right)^2}\right) - \qquad (1.12)$$

$$\frac{N_t}{8}(1 - F_c)\pi d_o^2.$$

The ideal pressure drop for the window zone (for Re > 100) is given by

$$\Delta p_w = \frac{2 + 0.6 N_{cw}}{2 S_m S_w \rho}\Gamma^2.$$

Two correction factors R_B and R_L can be interpolated from Figs. 1.14 and 1.15 or can be computed directly from

$$\begin{cases} R_B = 1 & \text{for } SS > 0.5 \\ R_B = \exp\left(-3.7\dfrac{S_b}{S_m}\left(1 - r_{ss}^{1/3}\right)\right) & \text{else} \end{cases}$$
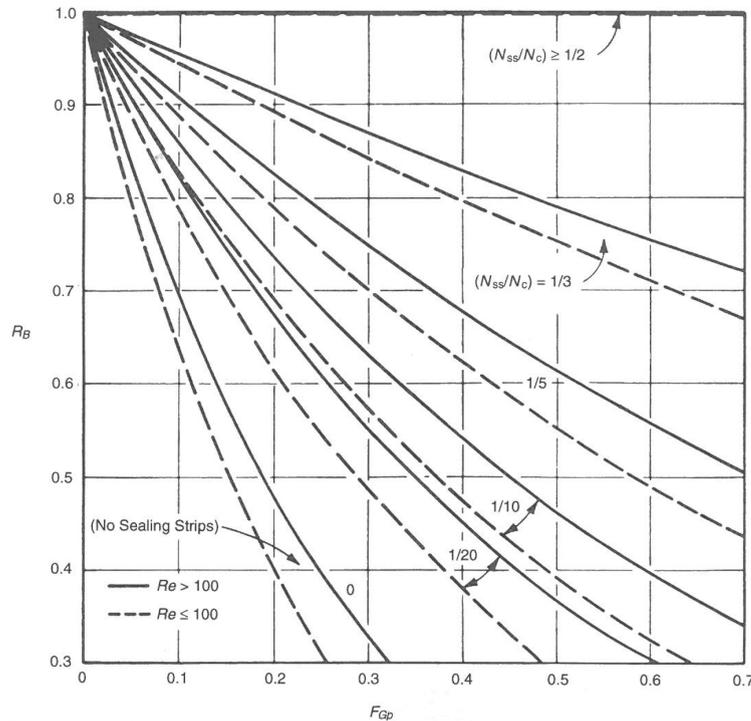
FIGURE 1.14. Correction factor for the influence of bypass on pressure drop [1]
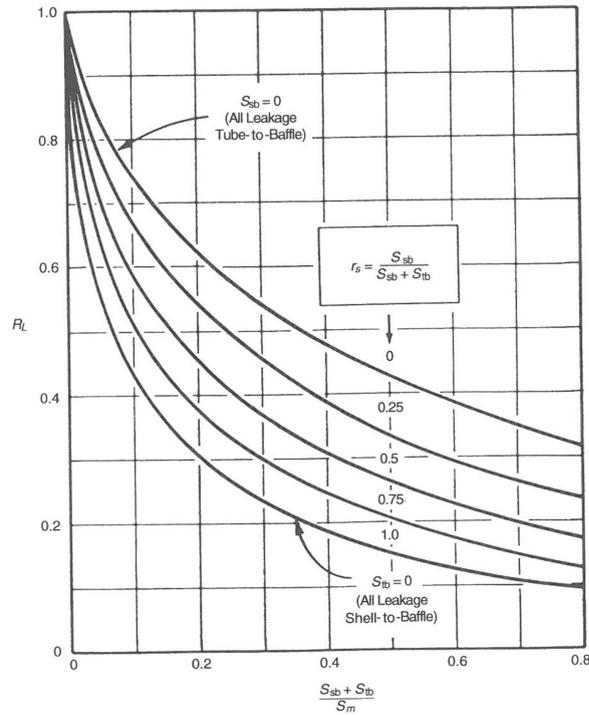
FIGURE 1.15. Correction factor for the influence of tube-to-baffle and shell-to-baffle leakage on pressure drop [1]

and

$$R_L = \exp\left(-1.33(1 + r_s)\right)\left(r_{lm}\right)^x.$$

Finally the **pressure drop across the shell** is given by

$$\Delta p_{\text{shellside}} = \left((N - 1)\,\Delta p_c R_B + N\Delta p_w\right) R_L + 2\Delta p_c R_B \left(1 + \frac{N_{cw}}{N_c}\right).$$

The Wills and Johnston method   The Wills and Johnston method is the simplified version of the so called flow stream analysis method and is suitable to hand calculations. The flow is separated into different paths, and to each fraction a mass flow Γ_i and a pressure drop Δp_i is assigned. Those paths can be recognized in Fig. 1.16: leakage between tubes and baffles (t), leakage between baffle and shell (s), crossflow over the tube bank (c) and bundle bypass flow (b).

The theoretical description of this method can be found in [1]; in the following the description of the method is provided with the correlations which are implemented in the software tool.
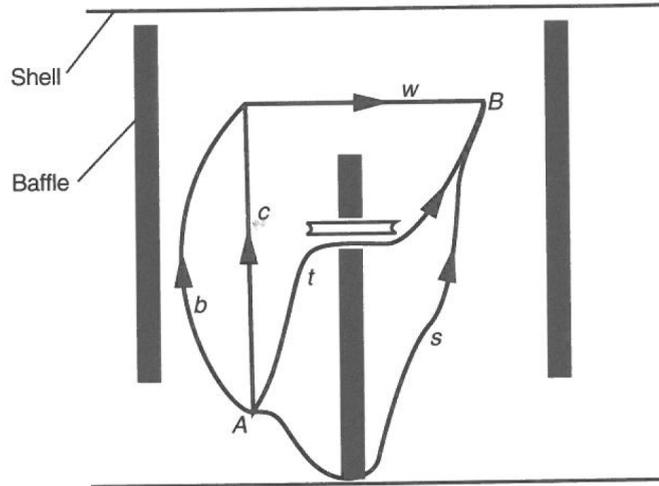
FIGURE 1.16. Flow streams in the Wills and Johnston method [1]

For each of the streams, a resistance coefficient n_i is defined such that the pressure drop is related to the mass flow

$$\Delta p_i = n_i \Gamma_i^2. \tag{1.13}$$

The pressure drop between the points A and B of Fig. 1.16 can then be expressed with the help of the coefficients n_i, with Γ_T being the total mass flow

$$\Delta p = n_p \Gamma_T^2$$
$$\Delta p_c = \Delta p_b = n_{cb} \Gamma_w^2$$

Calculation of the resistance coefficients n_i

1. The shell-to-baffle leakage area is calculated from

$$S_s = \pi \left(D_s - \frac{L_{sb}}{2} \right) \frac{L_{sb}}{2}.$$

The shell-to-baffle leakage resistance coefficient is given by

$$n_s = \frac{0.036 \left(2t_b / L_{sb} \right) + 2.3 \left(2t_b / L_{sb} \right)^{-0.177}}{2 \rho S_s^2}.$$

2. The tube-to-baffle leakage area is calculated from

$$S_t = N_t \pi \left(d_o - \frac{L_{tb}}{2} \right) \frac{L_{tb}}{2}.$$

The tube-to-baffle clearance resistance coefficient is given by

$$n_t = \frac{0.036\,(2t_b/L_{tb}) + 2.3\,(2t_b/L_{tb})^{-0.177}}{2\rho S_t^2}.$$

3. The window flow resistance coefficient is given by

$$n_w = \frac{1.9\exp\left(0.6856\frac{S_w}{S_m}\right)}{2\rho S_w^2}.$$

where S_m and S_w are the values defined in the Bell-Delaware method (Eqn. 1.6 and 1.12).

4. The bypass flow area is calculated from

$$S_b = L_{bb}L_{bc}$$

The bypass flow resistance coefficient is given by

$$\begin{cases} n_b = \dfrac{0.266 N_c N_{ss}}{2\rho S_b^2} & \text{for square layout} \\[2ex] n_b = \dfrac{0.133 N_c N_{ss}}{2\rho S_b^2} & \text{for triangular layout} \end{cases}$$

where N_c and N_{ss} are the same values used in the Bell-Delaware method (see Eqn. 1.8 and 1.9).

The coefficients n_s, n_t, n_w, n_b are assumed to be independent from the flow rate, therefore they can be calculated directly.

The coefficient n_c (crossflow resistance coefficient) varies with the flow rate, therefore it must be iterated as follows.

The fraction $F_{cr} = \Gamma_c/\Gamma_T$ represents the crossflow over total flow. Its value is used to compute the Reynolds number, defined for crossflow as:

$$\text{Re} = \frac{d_o}{\mu}\rho v_{\max} = \frac{d_o F_{cr}\Gamma_T}{\mu S_m}.$$

The crossflow resistance coefficient n_c is obtained by substituting

$$\rho v^2 = \frac{1}{\rho S_m^2}\Gamma^2$$

into Eq. 1.11, therefore:

$$n_c = \frac{N_c K_f}{2\rho S_m^2}.$$

The combined resistance coefficients are computed as:

$$n_{cb} = \left(n_c^{-1/2} + n_b^{-1/2} \right)^{-2} \qquad\qquad \text{bundle bypass and crossflow}$$

$$n_a = \left(n_w^{-1/2} + n_{cb}^{-1/2} \right)^{-2} \qquad\qquad \text{non leaking flow}$$

$$n_p = \left(n_a^{-1/2} + n_s^{-1/2} + n_t^{-1/2} \right)^{-2} \qquad\qquad \text{total flow coefficient}$$

the new value for F_{cr} is calculated by

$$F_{cr} = \left(\frac{n_p}{n_a} \right)^{1/2} \left[1 + \left(\frac{n_c}{n_b} \right)^{1/2} \right]^{-1}.$$

With the reasonable initial guess $F_{cr} = 0.5$, iterations are performed until F_{cr} converge.

Calculation of the flow fractions   The flow fractions can be then calculated:

$$F_b = \left(\frac{n_p}{n_a} \right)^{1/2} \left[1 + \left(\frac{n_b}{n_c} \right)^{1/2} \right]^{-1} \qquad\qquad \text{bypass flow}$$

$$F_s = \left(\frac{n_p}{n_s} \right)^{1/2} \qquad\qquad \text{shell-to-baffle leakage flow}$$

$$F_t = \left(\frac{n_p}{n_t} \right)^{1/2} \qquad\qquad \text{tube-to-baffle leakage}$$

Finally, **the heat transfer coefficient** can be calculated, using the corrected converged mass flow rate $\Gamma_c = F_{cr}\Gamma_T$, therefore

$$\mathrm{Re} = \frac{d_o F_{cr} \Gamma_T}{\mu S_m}$$

$$U_{\text{shellside}} = \frac{k}{d_o} 0.211 \, \mathrm{Re}^{0.651} \, \mathrm{Pr}^{0.34}$$

The pressure drop can be then calculated:

$$\Delta p = n_p \Gamma_T^2 \qquad\qquad \text{pressure drop per baffle space}$$

$$\Delta p_s = (N+1)\,\Delta p \qquad\qquad \text{total shell pressure drop}$$

1.3.1.3   HTC and Δp determination for the tubeside of the STHE

The determination of the heat transfer coefficient for a tube bundle follows the same procedure as for a single tube. In the following, all fluid properties are referred to the tubeside fluid, unless specified.

The front area of a single tube is given by

$$A_{\text{tube}} = \frac{\pi d_i^2}{4}.$$

The velocity in the tubes can be calculated from

$$A_{\text{front}} = A_{\text{tube}} \frac{N_t}{N_p}$$

$$v_{\text{tube}} = \frac{\Gamma}{A_{\text{front}}}$$

The mass flux on the tubeside is given by

$$\dot{M} = \frac{\Gamma}{A_{\text{front}}}$$

The Reynolds number and the Prandtl number are determined by

$$\text{Re} = \frac{d_i \dot{M}}{\mu}$$

$$\text{Pr} = \frac{c_p \mu}{k}$$

The correlation for the Nusselt number depends on the flow regime (i.e. the Reynolds number):

$$
\begin{cases}
\text{Nu} = 4.36^1 & \text{Re} < 2300: \text{Laminar flow} \\
\text{Nu} = \dfrac{f}{8} \dfrac{(\text{Re} - 1000)\text{Pr}}{1 + 12.7 \left(\frac{f}{8}\right)^{1/2} \left(\text{Pr}^{2/3} - 1\right)} & \text{Re} > 2300 : \text{Turbulent flow}
\end{cases}
\tag{1.14}
$$

where $f = (0.79 \ln(\text{Re} - 1.64))^{-2}$.

The used correlation for the turbulent flow regime in tubes is the Gnielinski correlation.

Finally the **tubeside heat transfer coefficient** is given by

$$
U_w = \frac{\text{Nu } k}{d_i}
$$

The **tubeside pressure drop** can be calculated with the help of the Blasius equation. $L_{\text{tube}} N_p$ is considered as the total length of a tube, excluding the bent sections.

$$
f_0 = 16/\text{Re} \qquad\qquad\qquad \text{for laminar flow}
$$
$$
f_0 = 0.079 \text{ Re}^{-1/4} \qquad\qquad \text{for turbulent flow}
$$
$$
\Delta p = 4 f_0 L_{\text{tube}} N_p \frac{\dot{M}^2}{2 d_i \rho}
$$

1.3.2   Printed circuit heat exchanger – Tool for design

Two arrangements for the channels of a printed circuit heat exchanger are possible. The most efficient, from a thermodynamical point of view, is the arrangement in counterflow (as shown in Fig. 1.17). Nevertheless a not negligible part of the channels is in crossflow, with a bended path inside the heat exchanger (as can be seen in the upper part of Fig. 1.17) in order to collect the fluids at the four different edges. The second option is the arrangement in complete crossflow, as described in Fig. 1.18. The two fluids follow straight channels, without any bending sections. This option is simpler to manufacture but less efficient from the heat exchange point of view. A tool is presented for the design of a PCHE in counterflow. A modeling tool for PCHE in crossflow can be found in [45].

---

[1] The Nusselt number for the case of laminar flow should be chosen in virtue of the nature of the heat transfer. Nu = 4.36 should be used for "convection with uniform surface heat flux" and Nu = 3.66, for "convection with uniform surface temperature". In order to be consistent with the values used by thermal hydraulic code TRACE, used in Chapter 2, the value for convection with uniform surface heat flux is proposed.
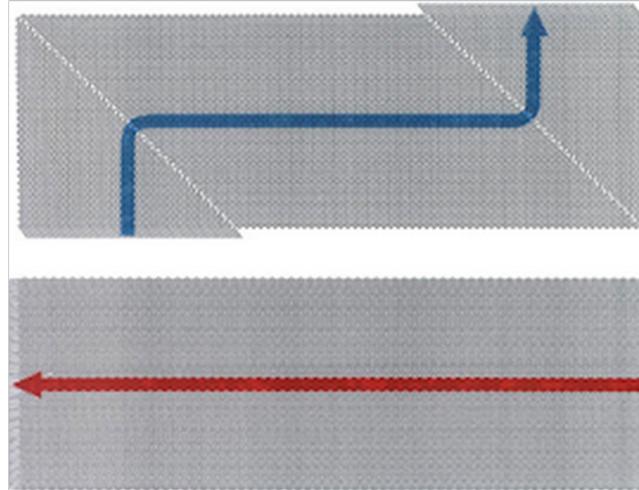
Figure 1.17. Two layers of a PCHE in counterflow, with bent sections at the top. [40]
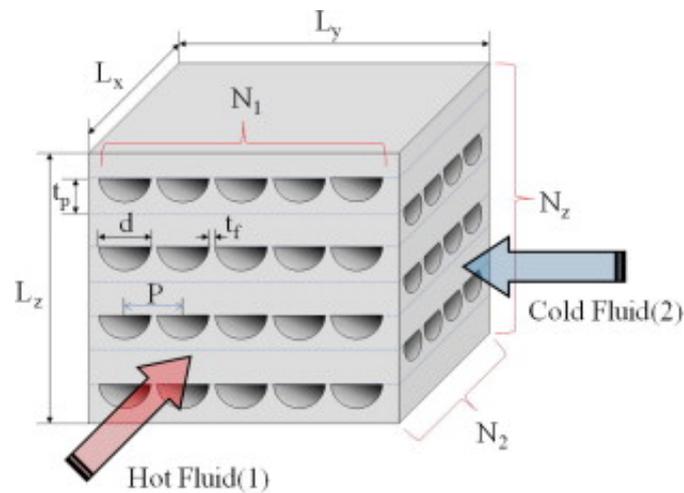
Figure 1.18. A schematic view of a PCHE in complete crossflow [45]

The PCHE in counterflow is modeled by considering a series of two semicircular channels separated by a slab, as shown in Fig. 1.7. The heat conduction across the metallic slab is analyzed further on, and takes into account the non rectangular shape of the structure. Heat conduction between channels not directly placed on top of each other was neglected. The bent sections (near the inlet and outlet) are approximated with straight channels, provided that the length of the heat exchanger is sufficiently large with respect to the width (at least by a factor of 3). The heat transfer in crossflow is neglected in this case.

The geometry of the PCHE in counterflow is determined following a similar approach to the modeling of the STHE. The logarithmic mean temperature ΔT_{LM} is determined as in Eq. 1.3 once the inlet and outlet temperatures of the two fluids are defined, without any correction factor, since the channel arrangement is considered as pure counterflow. The overall heat transfer coefficient UA is determined from the relation $Q = UA\Delta T_{\mathrm{LM}}$.

The free parameters to chose are the channel diameter d, the velocity in the channels v (limited to 5 m/s) and the ratio between the channel diameter and the plate thickness t_p. The pitch P between two horizontal channels is set to $1.1d$, which is a commonly found value in literature.

The cross sectional area for each fluid ($i = $ hot, cold) is determined using the volumetric flow rate $\dot{V}_i$ (obtained from $\dot{V}_i = \Gamma_i/\rho_i$) and the imposed velocity v

$$A_{\text{front},i} = \frac{\dot{V}_i}{v}.$$

counterflow printed circuit heat exchangers have the feature that the two cross sectional area relative to hot and cold fluid are equal, since the number of channels dedicated to the fluids must be the same. This is not the case for the PCHE in crossflow. The largest value for the area calculated above is chosen. This choice lowers the velocity of the other fluid, eliminating the risk of exceeding the upper limit for the velocity.

The number of channels for each fluid can be calculated from the total cross sectional area:

$$N_i = \frac{A_{\text{front}}}{A_{\text{channel}}},$$

where $A_{\text{channel}} = \pi d^2/8$. The total number of channels is $N = 2N_i$.

The dimensions of the heat exchanger in x and y direction can be calculated by

$$L_X = PN_i,$$
$$L_Y = t_p N_i.$$

After fixing the geometrical dimensions, the heat transfer coefficient can be calculated.

1.3.2.1   HTC and Δp determination of the PCHE

Several heat transfer correlations for non circular channels and different working fluids were presented in [45]. The heat transfer for molten salts was not investigated for semi-circular channels. In the present work the Gnielinski correlation for turbulent flow (for Re > 2300) and Nu = 4.36 for laminar flow are used (see Eq. 1.14), wshich are the most commonly found correlations in literature.

The heat transfer coefficient correlation for the two fluids is given by

$$U_i = \frac{\mathrm{Nu}_i k_i}{D_h} \quad i = 1, 2 \tag{1.15}$$

The heat transfer coefficient for the wall is given by

$$U_w = \frac{k}{t} \tilde{f} \tag{1.16}$$

where $\tilde{f}$ is a correction factor introduced to account for the geometry of the metallic plate and is described in the following section.

The heat transfer coefficient for the PCHE   is given by:

$$U = \left(\frac{1}{U_1} + \frac{1}{U_2} + \frac{1}{U_w} \right)^{-1} \tag{1.17}$$

After determining the heat transfer coefficient U from Eq. 1.17, the heat transfer area was calculated from $A_{\text{heat transfer}} = \frac{UA}{U}$, therefore the heat exchanger length

$$L = \frac{A_{\text{heat transfer}}}{(d + \pi d/2) \, N_i}.$$

The pressure drop across the channels of the PCHE is calculated with the correlation presented in [45] for semicircular channels:

$$\begin{cases} f_i = \dfrac{15.78}{\mathrm{Re}_i} & \mathrm{Re} < 2300 \\ f_i = 0.478 \, \mathrm{Re}^{-0.26} & 8200 < \mathrm{Re} < 58000 \end{cases}$$

$$\Delta p_i = 2 f_i \frac{L_i}{D_h} \rho_i v_i^2$$

The size of the heat exchanger can be finally determined by $L_X L_Y L$. The fluid volume in the exchanger is equal for both sides. It is calculated from

$$V = N_i L A_{\text{channel}}$$

1.3.2.2   HTC determination for the wall interface of a PCHE

The aim of this brief section is to describe the heat transfer in the metallic plate between two channels in the PCHE.

The relation between heat transfer coefficient for conduction and the geometrical/thermal properties of the material is given by

$$U_w = \frac{k}{t}\tilde{f}, \tag{1.18}$$

where k is the thermal conductivity and t is the thickness of the material across which the heat transfer takes place. The correction factor $\tilde{f}$ accounts for the non rectangular slab geometry of the metallic plate. The heat transfer coefficient across a rectangular slab depends linearly on the thickness t of the plate, without being influenced by the width. The temperature gradient is always perpendicular to the slab surface in the ideal case. In case of a semicircular slab (as shown in Fig. 1.19a), the heat transfer coefficient is influenced by both thickness and width. An analysis is conducted to determine the influence of the geometry on the heat transfer coefficient.

The heat equation to be solved is the Poisson equation $\vec{\nabla}\cdot(k\nabla T) = 0$. The thermal conductivity k is considered constant in the material, therefore the Poisson equation becomes Eq. 1.19. Neumann boundary conditions on the vertical axis (thermal insulation) and Dirichlet boundary conditions (imposed temperature) at the top and bottom of the geometry are chosen.

The heat flux $\dot{q}''$ is related by the Fick's Law to the temperature gradient via the thermal conductivity k. The third equation describes the heat flux via the heat transfer coefficient and the temperature difference across the solid (assuming a constant thermal conductivity in the material):

$$\begin{cases} \nabla^2 T = 0 \\ \left.\dfrac{\partial T}{\partial x}\right|_{x=0} = 0 \quad \left.\dfrac{\partial T}{\partial x}\right|_{x=d+t_f} = 0 \\ \left.T\right|_{y=0} = 0 \quad \left.T\right|_{\text{top}} = T_{\text{hot}} \end{cases} \tag{1.19}$$

The top part of the metallic plate is parameterized as

(A) Real geometry   (B) simplified geometry
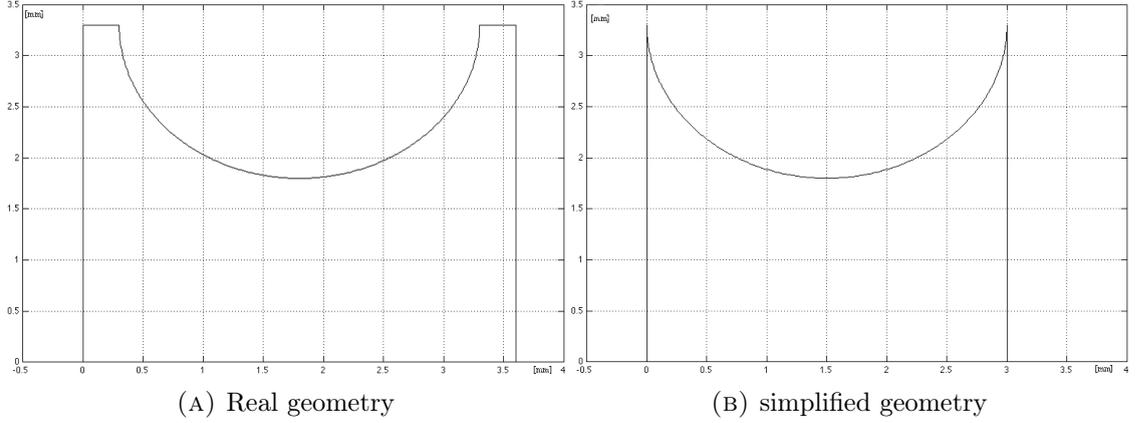
FIGURE 1.19. Metallic plate geometry between two semicircular channels

$$y = \begin{cases} t_p & 0 < x < t_f/2 \\ t_p - \sqrt{d^2 - x^2} & t_f/2 < x < t_f/2 + d \\ t_p & t_f/2 + d < x < t_f + d \end{cases}$$

with $x \in [0, d + t_f]$, with the definition of the symbols as in Fig. 1.18.

The heat flux $\dot{q}''$ is determined locally by the conductivity k and the temperature gradient ∇T. The average heat flux $\dot{q}''_{av}$ is expressed in terms of the temperature difference ΔT between the top and bottom of the plate and a heat transfer coefficient U:

$$\dot{q}'' = k\nabla T \tag{1.20}$$

$$\dot{q}''_{av} = U_w \Delta T \tag{1.21}$$

As a first step, the heat transfer problem was solved for a simplified geometry, where t_f is set to 0. The geometry becomes as shown in Fig. 1.19b and depends only on two parameters: the width d and the height (thickness) t_p of the plate.

The heat transfer coefficient U is the parameter which needs to be determined. The independent quantities of the problem are: the length (m), the temperature (K) and the thermal conductivity expressed in W/m·K (the power in W is the independent quantity). The degrees of freedom of the problem can be reduced by using non-dimensional variables.

A *characteristic length* t_p is introduced such that the non-dimensional length is defined as $\tilde{x} \equiv \frac{\vec{x}}{t_p}$. The temperature is scaled with the characteristic temperature T_{hot} as $\theta \equiv \frac{T}{T_{\text{hot}}}$. The heat transfer coefficient U_w can be expressed in an non-dimensional form: $\tilde{U}_w \equiv U_w \frac{t_p}{k}$.

The scaling of variables for the infinitesimal terms in Eq. 1.19 and 1.20 results in:

$$d\vec{x} = t_p d\tilde{\vec{x}}$$

therefore the laplacian operator is

$$\nabla^2 = \frac{1}{t_p^2}\tilde{\nabla}^2.$$

Finally, the non-dimensional form of Eq. 1.19 is expressed as

$$\begin{cases} \dfrac{\Delta T}{t_p^2}\tilde{\nabla}^2\theta = \tilde{\nabla}^2\theta = 0 \\[2ex] \left.\dfrac{\partial\theta}{\partial\tilde{x}}\right|_{\tilde{x}=0} = 0 \quad \left.\dfrac{\partial\theta}{\partial\tilde{x}}\right|_{\tilde{x}=d/t_p} = 0 \\[2ex] \left.T\right|_{\tilde{y}=0} = 0 \quad \left.T\right|_{\text{top'}} = T_{\text{hot}} \end{cases} \tag{1.22}$$

where the non-dimensional parameterization of the upper part of the simplified geometry is expressed as

$$\tilde{y} = 1 - \sqrt{\left(\frac{d}{t_p}\right)^2 - \tilde{x}^2} \qquad 0 < x < d/t_p \tag{1.23}$$

Equation 1.20 and 1.21 become:

$$\tilde{\dot{q}''} \equiv \dot{q}''\frac{t_p}{k\Delta T} = -\tilde{\nabla}\theta \tag{1.24}$$
$$\tilde{U}_w = -\tilde{\nabla}\theta \tag{1.25}$$

The parameterization of the geometry of the system depends only on the ratio d/t_p, while Eq. 1.22, 1.24 and 1.25 are non-dimensional equations. The non-dimensional heat transfer coefficient is therefore function of the ratio between the channel diameter and the plate thickness d/t_p. This is the main result of this non-dimensional analysis.

Once the relation $\tilde{U}_w = \tilde{f}\left(\frac{d}{t_p}\right)$ is found, the heat transfer coefficient U_w can be found with Eq. 1.18.

An analytical solution of the Poisson equation (1.19) could not be found for the considered geometry, therefore a numerical approach is followed. The heat equation is solved numerically by the PDE toolbox present in Matlab. The boundary condition T_{hot} is set

to 100°. The temperature gradient ∇T is calculated at the bottom of the plate and plotted for different geometry configurations (see Fig. 1.20). The non-dimensional heat transfer coefficient can be fitted with a polynomial function $\tilde{f}$:

$$\tilde{f}\left(\frac{d}{t_p}\right) = 0.4499 \left(\frac{d}{t_p}\right)^2 + 0.3403 \left(\frac{d}{t_p}\right) + 1 \qquad (1.26)$$
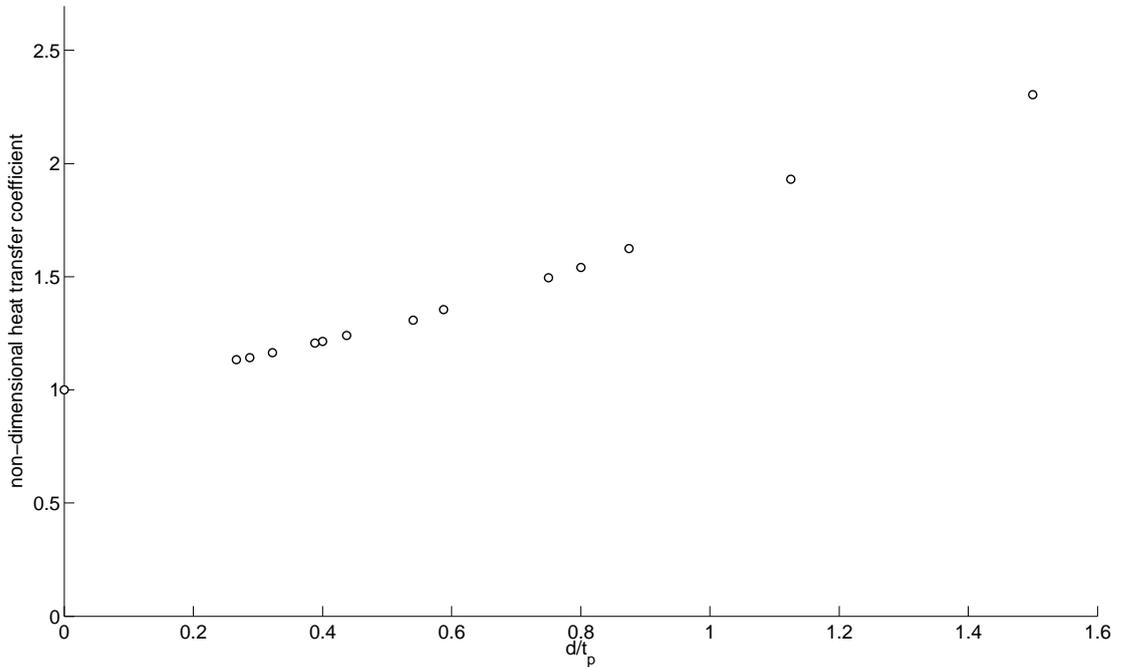
FIGURE 1.20. $\tilde{U}$ as function of d/t_p. The numerical solution obtained with Matlab of Eq. 1.22 for different geometrical configurations were plotted as function of d/t_p.

Typical values for the d/t_p ratio used in PCHE are around 1. The heat equation is then solved with Matlab for *real geometrical* , applying the relation $t_f = 0.1d$, which is in the range of the values found in literature. The difference between the interpolated result and the result obtained from the solution from Matlab is maximal 1.5% for the non-dimensional heat transfer coefficient. For $t_f = 0.2d$ it is maximal 2.5%. Therefore the correlation for the non-dimensional heat transfer coefficient for the simplified geometry holds also in the real geometry case, without the need of introducing a correction factor.

1.4   Preliminary design of the MSFR primary heat exchanger

The reactor design of the Molten salt fast reactor (MSFR) was proposed in the frame of the EVOL project, and includes a fairly detailed description of the core, few specifications about the out-of-core part of the primary circuit and a description of the fuel salt

properties [3].

The MSFR core parameters are summarized in Tab. 1.3.

TABLE 1.3. MSFR core parameters [6]

Thermal power $\dot{Q}$	[MW]	3000
Core inlet temperature	[K]	923
Core outlet temperature	[K]	1023
Fraction of salt inside the core	[-]	50%
Number of loops for heat exchange	[-]	16

The software tool described previously is applied to the constraints of the design of the MSFR. A preliminary design for shell and tube heat exchanger and a printer circuit heat exchanger in counterflow are obtained with the developed tool and are presented in the next section.

1.4.1 Input parameters and constraints

In the design of the MSFR sixteen heat exchangers are responsible for the heat transfer of the 3000 MW$_{\text{th}}$ from the primary to the intermediate circuit. Each unit transfer 187.5 MW$_{\text{th}}$.

The primary salt containing the fuel was chosen to be an eutectic mixture of LiF-ThF$_4$ with molar fractions 0.775-0.225. The thermophysical properties of the primary salt can be found in Tab. 1.4.

TABLE 1.4. Thermophysical properties for the primary salt [4]

		LiF-ThF$_4$ 0.78-0.22
T_{melting}	[K]	838
T_{boiling}	[K]	1874
ρ	[kg/m^3]	$4983.56 - 0.882 \cdot T$
μ	[mPa·s]	$\rho \left(5.54 \cdot 10^{-5} \exp \left(3689/T \right) \right)$
k	[W/m·K]	$0.928 + 8.397 \cdot 10^{-5} \cdot T$
c_p	[J/kg·K]	$-1111 + 2.78 \cdot T$

The total volume of salt flowing through the core is 18 m^3, while the fraction in the heat exchangers is approximately 34% (6.12 m^3) [3]. The volume of the primary salt in each heat exchanger is limited to 0.38 m^3. For the preliminary analysis of a single heat exchanger a limiting volume for the primary and intermediate salt of 0.33 m^3 is chosen as a constraint.

The intermediate salt temperatures have to be determined given the constrained inlet and outlet temperatures for the primary salt. Eq. 1.1 relates the overall heat transfer coefficient UA to the power Q and to the logarithmic mean temperature ΔT_{LM}. In order to achieve a reasonable design from an engineering point of view, the heat transfer area A, therefore the dimensions (and costs) of the heat exchanger need to be limited. This choice results in a low value for the overall heat transfer coefficient UA. Thus a large value for ΔT_{LM} is consequently required, which is obtained with low intermediate salt inlet and outlet temperatures. On the other hand the efficiency of power cycle is determined by a high temperature of the working fluid. Therefore the temperature of the intermediate salt – which gives up the heat to the working fluid of the power cycle – should be kept high, limiting ΔT_{LM} at the top.

The primary salt temperatures are fixed for inlet and outlet at 1023 K and 923 K by design. A safety requirement for the intermediate salt temperature is to be always above the freezing temperature of the primary salt: 838K. A safety margin of 20K was added to the freezing temperature of the primary salt, choosing the inlet temperature for the intermediate salt to be 863 K (590°C).

The intermediate salt outlet temperature is chosen to be a free parameter to be varied. Different heat exchanger configurations depending on the intermediate salt outlet temperatures are investigated. A high intermediate salt outlet temperature would result in a better thermal efficiency in the power production cycle, but other parameters need to be considered, such as velocity in the pipes and pressure drops in the intermediate circuit.

The maximal velocity in each section of the heat exchanger needs to be limited to 5 m/s to avoid erosion and corrosion [3]. A higher velocity increases the Reynolds number and therefore improves the heat transfer in case of turbulent flow regime, but due to the erosive salt properties the velocity must be limited to protect the piping system.

The intermediate salt was not defined in the frame of the EVOL project for the MSFR. Two different salts are investigated in this work, regarding thermophysical properties only. The salts are LiF-BeF$_2$ (0.66-0.34), which was the intermediate salt used for the MSRE, and LiF-NaF-KF (0.465-0.115-0.42). An exhaustive description of the salts can be found in the work of Beneš [18]; thermophysical properties used in this work are listed in Tab. 1.5.

The pressure drops for primary and intermediate salts need to be kept as low as possible. Low pressure drops reduce the energy requirement for the pumping systems, increasing the overall efficiency of the plant. For the MSFR the pressure drop for the primary salt should be low enough to assure natural circulation in case of a loss-of-flow accident. In

TABLE 1.5. Thermophysical properties for the intermediate salts [18]

		LiF-NaF-KF 0.465-0.115-0.42	LiF-BeF$_2$ 0.66-0.34
T_{melting}	[K]	727	728
ρ	[kg/m^3]	$2579.3 - 0.6240 \cdot T$	$2146.3 - 0.4884 \cdot T$
μ	[mPa·s]	$0.0248 \exp\left(4477/T\right)$	$0.116 \exp\left(3755/T\right)$
k	[W/m·K]	$0.36 + 5.6 \cdot 10^{-4} \cdot T$	1.1
c_p	[J/kg·K]	1880	2390

case of stagnation of flow the decay heat in the primary circuit – in particular in the heat exchanger – could increase the temperatures locally and damage the structural materials.

For a preliminary design no maximal pressure drop is defined a priori. Among all possible solutions, the design with lowest pressure drop is chosen for further investigations.

The metal chosen for the preliminary design of the heat exchanger was Hastelloy® N alloy. Hastelloy® N is a nickel-base alloy developed by ORNL and the International Nickel Company for use in molten-salt reactors [13, 46]. It was used for the primary heat exchanger in the MSRE. The experiment did not show fouling of the heat exchanger during three years of operation, due to scale build up or corrosion of the internals [14]. No detriment of the heat transfer was proved. Hastelloy® N alloy is therefore a strong candidate to be used for the primary heat exchanger of the MSFR. Its physical, chemical and mechanical properties are described in [46]. In Tab. 1.6 the properties are listed for $T = 923$ K. The constraints of the problem are summarized in Tab. 1.7.

TABLE 1.6. Hastelloy® N alloy properties [46]

Melting temperature	[K]	1573 - 1673
Mean coefficient of thermal expansion	[m/m·K]	14.7
Thermal conductivity	[W/m·K]	23.6
Specific heat	[J/kg·K]	578

TABLE 1.7. Constraints for one modular primary heat exchanger for the MSFR.

Q	[MW$_{\text{th}}$]	187.5
$T_{F,\text{in}}$	[K]	1023
$T_{F,\text{out}}$	[K]	923
$T_{C,\text{in}}$	[K]	863
v_{max}	[m/s]	5
$V_{\text{primary salt, max}}$	[m^3]	0.33

1.4.2   Shell and tube heat exchanger

The first step described in Sec. 1.3.1 for the preliminary design of the STHE is the estimation of the heat transfer coefficient U_{est}. The heat transfer coefficient found experimentally for the shell and tube heat exchanger of the MSRE in the 1960s was 3725 W/m^{2}K. Due to the lack of experience and following a conservative approach, a value of $U_{est} = 3000$ W/m^{2}K is chosen. The conservative approach (lower estimated heat transfer coefficient) results in a larger required area A_{req}.

The allocation of the fluids in a shell and tube heat exchanger depends on several factors, as pressure difference between the fluids, limiting pressure drops, fouling, corrosion rates, phase change, etc. A rule-of-thumb is the allocation of the high pressure fluid on the tubeside. This allows to use a smaller shell thickness, since the shell does not need to sustain a high pressure from the inside. The two salts of the MSFR flow at the same near atmospherical pressure, therefore this first criteria is applicable. In case the pressure drop for one specific fluid need to be kept low, this fluid should be placed in the shellside. The minimization of the pressure drops is more relevant for the primary circuit, therefore the primary salt should be allocated in the shellside. The other mentioned criteria are not relevant for the allocation of the fluids, since the behavior is expected to be similar for both salts. Besides this motivation, the same approach was used for the STHE of the MSRE in the 1960s, therefore the primary salt is allocated in the shellside, the intermediate salt in the tubeside.

In order to decrease the size of the heat exchanger the shellside salt volume the most compact tube layout is chosen: triangular tube arrangement. A triangular tube arrangement increases the velocity of the shellside fluid, enhancing the heat transfer by increasing the Reynolds number.

The thickness of the tubes is fixed to 0.8 mm. At first this value could be considered to be small, but considering that the salts are flowing at similar pressures this thickness can be sufficient. A small tube thickness decreases the thermal resistivity of the metal, improving the heat transfer through the wall. The heat transfer coefficient for the shell and tube heat exchanger will be then influenced mostly by the flow properties of the salts, as described by Eq. 1.5.

The variables free to choose in the software tool for the design of a shell and tube heat exchanger are the outer diameter d_o, the number of passes N_p, the maximal velocity in the tubes v_{max} and the outlet temperature for the intermediate salt $T_{C,out}$. The range for each variable is listed in Tab. 1.8, each possible combination was investigated.

TABLE 1.8. Range of input values for the STHE

d_o	[mm]	$3 - 40$
$v_{\max}$	[m/s]	$1 - 5$
N_p	[-]	2, 4, 6
$T_{C,\text{out}}$	[K]	$903 - 953$

No geometrical configuration for a shell and tube heat exchanger respecting the above mentioned criteria and constraints are found.

Several geometrical configurations deliver the required overall heat transfer coefficient UA, but the constraints on the salt volume could not be respected following the design standards of TEMA. The primary salt is placed in the shellside, following the approach used during the MSRE. The limitation on the primary salt volume in the heat exchanger (0.34 m^3) forced a very compact tube arrangement. The tube pitch is decreased and the most compact tube layout (triangular) is chosen. Consequently the minimal flow area for the primary salt decreased. The velocity is inversely proportional to the flow area and exceed its upper limit (5 m/s).

Besides this, even by exceeding the limits on the salt volume (in this example of design the shellside volume is 1 m^3), the manufacturing the STHE seems to be unrealistic for the imposed constraints. One possible solution obtained from the tool imposed a very small outer diameter of the tubes ($d_o = 7$ mm), a number of tubes of the order of 25'000 and a length of 2 m. The maximal velocity in the shellside is respected (4 m/s), as well as the overall heat transfer coefficient requirement. For the design of a STHE the minimal tube diameter proposed in [36] is 1 cm with a tube thickness of 1.2 mm. In virtue of these considerations, this type of heat exchanger poses manufacturing limitations for the application on the MSFR. The shell and tube heat exchanger is therefore discarded for further analysis, under the design conditions of the EVOL project.

1.4.3 Printed circuit heat exchanger

The developed model for design of a PCHE is applied to the parameters and constraints of the MSFR. Different configurations for the channel length and the height of the HX are found, leading to the required low salt volume and overall heat transfer coefficient. The channel length is directly proportional to the pressure drop. A shorter length is wished to limit the energy requirement for pumping and improving natural circulation in case of accident. On the other hand a design of a tall and short heat exchanger is excluded due to space limitations surrounding the reactor. Both aspects are considered

for the choice of the primary heat exchanger of the MSFR, and the designs for both investigated intermediate salts are listed in Tab. 1.9.

For both cases a laminar flow regime is achieved, due to a very small channel diameter (approximately 1.5 mm and velocities limited to 2 m/s. The heat transfer coefficient is velocity independent (laminar flow), therefore the ability of the HX to exchange heat is expected to depend only on the temperature difference (ΔT_{LM}) between the two fluids. This aspect becomes relevant in case of a loss-of-flow accident.

The counterflow arrangement theoretically allows to reach a very high thermal efficiency (i.e. an outlet temperature of the intermediate salt close to the inlet temperature of the primary). For the case of the MSFR a compromise between thermal efficiency and thermal hydraulic efficiency (pressure losses) has to be achieved, therefore the intermediate salt outlet temperature is fixed to 943 K. The thermal effectiveness is the ratio of at the actual to the maximum heat transfer rate $E = \dot{Q}/\dot{Q}_{\mathrm{max}}$, and can be expressed [1] as

$$E = \frac{T_{c,\mathrm{out}} - T_{c,\mathrm{in}}}{T_{h,\mathrm{in}} - T_{c,\mathrm{in}}},$$

with the nominal temperatures and flow rates the effectiveness is 50% (for typical heat exchangers lies in the range 40% to 80%). The logarithmic mean temperature difference is $\Delta T_{\mathrm{LM}} = 69.52$ K.

The design is similar for the two heat exchangers with different intermediate salt (the geometrical parameters differs approximately by 10%). The salt properties, in particular the viscosity, affect the Reynolds number and therefore the pressure drop of the salts. The viscosity of FliBe ($7.42 \cdot 10^{-3}$ Pa·s) is twice the viscosity of FliNaK ($3.53 \cdot 10^{-3}$ Pa·s), which determines a low pressure drop of the FliNaK salt in the primary heat exchanger.

1.5 Preliminary design of the MSFR intermediate heat exchanger

In the next chapter the behavior of the primary heat exchanger wants to be investigated with thermal hydraulic code TRACE. In order to perform this analysis the intermediate circuit must be closed, with the help of an intermediate heat exchanger.

The simplicity of the model for the design of the PCHE for the primary heat exchanger, together with the good thermal efficiency, makes the PCHE a suitable candidate also for the intermediate heat exchanger.

TABLE 1.9. Preliminary design of the primary PCHE in complete counterflow

		LiF-BeF$_2$	LiF-NaF-KF
Width	[m]	0.29	0.27
Height	[m]	4.57	5.32
Length	[m]	1.17	1.09
Channel diameter	[mm]	1.7	1.6
Channel pitch	[mm]	1.9	1.8
Plate thickness	[mm]	1.4	1.3
Channels	[#]	253356	307589
U_1	[W/m^2·K]	2.24E3	4.50E3
U_2	[W/m^2·K]	4.62E3	3.86E3
U_W	[W/m^2·K]	3.37E4	3.59E4
U	[W/m^2·K]	2.07E3	1.96E3
A	[m^2]	1300	1373
UA	[W/K]	2.70E6	2.70E6
$T_{\mathrm{in},1}$	[K]	1023	1023
$T_{\mathrm{out},1}$	[K]	923	923
$T_{\mathrm{in},2}$	[K]	863	863
$T_{\mathrm{out},2}$	[K]	943	943
Re$_1$	[-]	494	432
Re$_2$	[-]	477	1117
v_1	[m/s]	1.17	1.08
v_2	[m/s]	2.00	2.00
Δp_1	[bar]	4.1	4.0
Δp_2	[bar]	5.2	2.6
Salt volume	[m^3]	0.34	0.34

1.5.1   Working fluid in the power production cycle

High temperature cycles are currently used in industry for power production and process heat (e.g. desalination, synthetic and unconventional oil production, oil refining, etc. [52]). Different working fluids can be employed, depending on the required duty, temperature range and working environment.

Molten salts are employed as heat transfer fluids in Concentrated Solar Power (CSP) plant. Focussed sunlight is directed on pipes with circulating molten salt. The molten salt is pumped through heat exchangers where it releases heat to produce steam. Steam produced with CSP can reach 855 K (585°C) at a pressure of 155 bar, which is converted through a steam turbine into mechanical energy (state-of-the-art technology for CSP produce 250 MW[30]).

Other options as working fluid in the power production cycle are investigated for the MSFR: the helium Brayton cycle, the supercritical CO$_2$ cycle and supercritical water

cycle, which has higher efficiency compared to superheated steam. The feasibility of a power cycle with the proposed fluids in terms of state-of-the-art technology, thermal efficiency and manufacturing experience was researched in literature.

Dostal et al. [22] investigated supercritical CO_2 (sCO_2) as working fluid for the new generation of nuclear reactors, using a printed circuit heat exchanger. A higher thermal efficiency (approaching 53%) with respect to conventional Rankine steam cycles is an attractive feature for high temperature reactors. Supercritical CO_2 was selected among other gases (e.g. SO_2, N_2O_4 and NO_2) because of the moderate value of its critical pressure, its stability and relative inertness (for the temperature range of interest), sufficient knowledge of its thermodynamic properties, non-toxicity, abundance and low cost[22]. The critical conditions of CO_2 are achieved at 73.8 bar and 304.1 K. Despite this, the high temperature of the gas pose a technological limit on the turbine. Supercritical CO_2 is very corrosive at temperatures above 715 K [47], and the materials available for a turbine can not withstand a such corrosive environment. The use of supercritical CO_2 seams to be therefore not suitable for application in high temperature reactors.

A helium Brayton cycle has the same efficiency as a supercritical CO_2 cycle for gas temperatures above 1123 K. The operating pressure for the helium Brayton cycle is much higher than for supercritical CO_2 (200 bar)[22]. In the temperature range of the MSFR the efficiency of a helium cycle drops, due to the large energy investment needed to pressurize the fluid with respect to the energy gain. Helium is therefore discarded as heat sink of the modeled system.

Supercritical water has been used throughout the years for power production. State-of-the-art supercritical steam power plant in Lünen [29] was commissioned by Siemens and is in operation since 2013. This hard-coal-fired power plant has an installed electrical capacity of 750 MW, with almost 46% efficiency. The steam parameters at the boiler outlet reach 280 bar and 610°C. The MSFR reaches temperatures in the range of the steam parameters of this coal-fired power plant. Supercritical water appear therefore suitable for an application to the power cycle in the MSFR.

In this thesis work the working fluid for the power cycle is used as balance of plant, representing the heat sink of the system. The modeling of the heat exchangers aims at ensuring a high efficiency of the plant, therefore a high outlet temperature of the working fluid, but the modeling of the power generating cycle is not part of this thesis. Supercritical water is selected as the working fluid for the balance of plant, and the design of the intermediate heat exchanger is presented in the next section.

1.5.2   Printed circuit heat exchanger

The goal of the design of an intermediate heat exchanger is to allow the simulation with thermal hydraulic code TRACE of the behavior of the system in steady state and accident conditions. The pressure of supercritical water is set to 225 bar. The inlet temperature is set to 800 K, far above the freezing point of the salts. This avoids a priori freezing in the primary and intermediate circuit.

No thermal losses are considered in the intermediate circuit, therefore the intermediate salt temperatures are already determined by the primary heat exchanger. The flow rate of the intermediate salt is determined by the heat transfer modeling of the primary heat exchanger.

The technology of a PCHE allows two fluids at different pressures [40], making it a good candidate also for the intermediate heat exchanger of the MSFR.

The previously described design tool for PCHE in counterflow is adapted to the present case. No constraints for the salt volume are imposed, since a larger volume could considered positive from a safety point of view, due to the large thermal inertia in the intermediate circuit.

The water velocity is limited to 10 m/s. The water outlet temperature is a free parameter of the tool and was set to approximately 910 K (depending on the choice of the intermediate salt), which is the temperature limited by current technological limits of the turbine. Regarding dimensions, velocities and pressure drops the most favorable design is chosen.

Tab. 1.10 lists the geometrical and thermal hydraulic parameters of the intermediate heat exchanger for two different salt configurations.

TABLE 1.10. Preliminary design of the intermediate PCHE in complete counterflow

		LiF-BeF$_2$	LiF-NaF-KF
Width	[m]	0.90	0.96
Height	[m]	5.33	5.2
Length	[m]	2.69	2.88
Channel diameter	[mm]	5	5
Channel pitch	[mm]	5.5	5.5
Plate thickness	[mm]	4.2	4.2
Channels	[#]	104175	108998
U_2	[W/m^2·K]	1.57E3	1.24E3
U_{water}	[W/m^2·K]	7.74E3	7.74E3
U_W	[W/m^2·K]	1.15E4	1.15E4
U	[W/m^2·K]	1.17E3	9.748E2
A	[m^2]	3597	4038
UA	[W/K]	4.22E6	3.94E6
$T_{\text{in},2}$	[K]	863	863
$T_{\text{out},2}$	[K]	943	943
$T_{\text{in},W}$	[K]	800	800
$T_{\text{out},W}$	[K]	913	908
Re$_2$	[-]	395	1009
Re$_{\text{water}}$	[-]	47619	47619
v_2	[m/s]	0.56	0.58
v_{water}	[m/s]	8.00	8.00
Δp_2	[bar]	0.4	0.2
Δp_{water}	[bar]	0.4	0.4
Salt volume	[m^3]	2.75	3.08

1.6   Conclusions

A preliminary choice for primary heat exchanger for the Molten Salt Fast Reactor was performed in the first part of this chapter. Among different options and designs two types of heat exchanger were chosen for a preliminary analysis, based on temperature, pressure and operational conditions of the MSFR, together with the state-of-the-art technology and manufacturing experience with heat exchangers. Shell and tube heat exchangers and printed circuit heat exchangers were chosen as possible candidates for the MSFR.

A software tool was *ad hoc* developed with MATLAB for the design of the two types of heat exchanger respecting the constraints of the MSFR. Two different intermediate salts (FliBe and FliNaK) were tested in virtue of their different thermophysical properties.

The analysis demonstrated the impossibility to use a traditional shell and tube heat exchanger for the MSFR, following the guidelines and the construction standards of the TEMA. The approach used during the MSRE for the placement of the primary salt in the

shellside was followed. The limitation on the primary salt volume in the heat exchanger (0.34 m^3) forced a very compact tube arrangement. Consequently the minimal flow area for the primary salt decreased, and the velocity (inversely proportional to the flow area) exceed its upper limit.

The design of a printed circuit heat exchanger for the primary heat exchanger obtained with the MATLAB tool fulfilled the criteria of the MSFR. Two designs were proposed according to the properties of two intermediate salts. The main feature of PCHE is the very small diameter of the semicircular channels (1.6 mm for the design with FliBe as intermediate salt). This determines a very large heat transfer area per unit volume, which decreases the overall size of the HX ($0.29 \times 1.17 \times 4.57$ m). The intermediate outlet temperature of the salt is set to 943 K balancing the thermal effectiveness and the thermal hydraulic constraints.

In order to close the intermediate circuit for the simulation with TRACE in the following chapter, a second heat exchanger was designed. For sake of simplicity the intermediate heat exchanger was chosen to be a PCHE, with similar characteristics to the primary HX. Different working fluids for the power circuit were briefly investigated, opting finally for supercritical water. Two designs (for two intermediate salts FliBe and FliNaK) for the intermediate heat exchanger were proposed. The supercritical water temperature at the outlet of the PCHE is 913 K, leading to temperature drop between core and power circuit of 110 K.

Chapter 2

Modeling and analysis of the primary and intermediate circuit of the MSFR in steady state and accidental conditions

2.1 Introduction

In the previous chapter a preliminary design regarding type, dimensions, flow rates and temperatures of the fluids for the primary and intermediate heat exchanger of the MSFR was proposed. Two different intermediate salts (LiF-Be$_2$ and LiF-NaF-KF) were investigated; according to their properties two pairs of heat exchangers were modeled.

The aim of this section is to model the primary, intermediate and heat sink circuit with thermal hydraulic code TRACE. First the two above mentioned configurations are modeled in TRACE and optimized for steady state conditions. In the second part of this chapter the behavior of the system is investigated under accidental conditions (unprotected station-black-out SBO). Different configurations for the primary, intermediate and heat sink circuit are investigated.

The primary circuit was modeled in TRACE following the constraints of the MSFR proposed design. For the intermediate circuit a previous analysis could not be found in literature, therefore a similar approach to the primary circuit is used.

2.2 TRACE modeling

As a first step, physical and thermodynamical properties of the salts have been implemented in TRACE. The correlations for the properties can be found in Chapter 1 in Tab. 1.4 and 1.5 and are taken from the works of Beneš [18] and Rouch [4]. The strong temperature dependence of the linear correlation for the heat capacity of the primary salt created instabilities in the code. Therefore the correlation was replaced with the averaged value over the validity range of the correlation (867-907 K): $c_p = 1355$ J/kg·K. Beneš proposed, on the basis of the comparison between the ideal heat capacity and the measured data from other fluoride systems taken from the work of Powers et al. (Nucl. Sci. Eng, 1963, 71), the value $c_p = 1000$ J/kg·K [18].

The material chosen for the heat exchanger is Hastelloy® N. In TRACE materials can be defined by a temperature dependent table with density, heat capacity, thermal conductivity and emissivity. The properties of Hastelloy® N (listed in Tab. 1.6) are added to the TRACE model.

As described in the previous chapter, the geometry of the heat structure is not a rectangular slab, but a structure separating two semicircular channels. A correction factor $\tilde{U}_w = f\left(\frac{d}{t_p}\right)$ (non-dimensional heat transfer coefficient) is introduced to model correctly the heat transfer in the structure. This correction factor depends on the ratio between the diameter of channel and heat structure thickness. The heat transfer coefficient can be then expressed as

$$U_w = f\left(\frac{d}{t_p}\right)\frac{k_w}{t_p}.$$

Different types of Hastelloy® N are generated by creating an equivalent thermal conductivity ($k_{w,\,eq} = f\left(\frac{d}{t_p}\right)k_w$). Depending on the desired ratio, a specific type of Hastelloy® N is used for the simulation in TRACE. This expedient allows to maintain the correct thermal inertia of the heat structure and simultaneously to model correctly the heat transfer. This modeling approach is relevant for the simulation of accidental conditions, where the thermal inertial of the metal is expected to have a significant role.

2.2.1 Steady state

2.2.1.1 Primary heat exchanger

At first the performance of the primary heat exchanger in steady state conditions is investigated using TRACE. A single pair of channels is separated by a heat structure

of the desired geometrical dimensions and thermal conductivity, based on the results
from the preliminary design (see Tab. 1.9). A multiplication factor representing the
total number of channels is applied to the model. The inlet temperatures and the mass
flow rates are fixed through boundary conditions (component *fill* and *break*). The heat
exchange is investigated in counterflow conditions. A schematic view of this simple circuit
can be seen in Fig. 2.1.
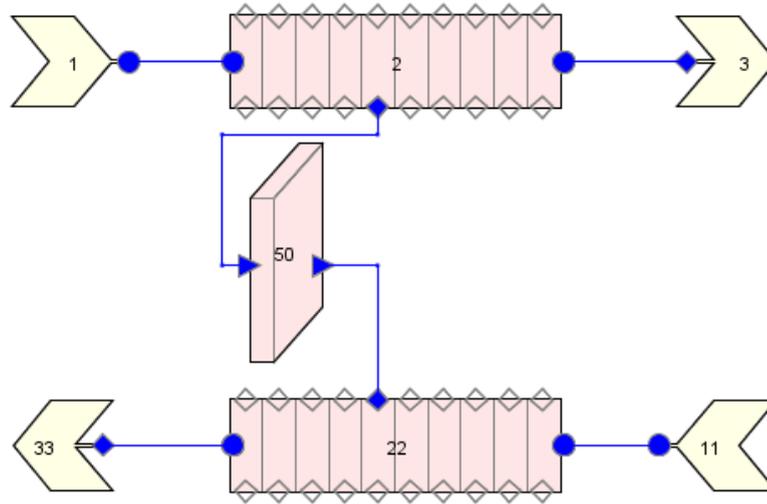
FIGURE 2.1. Simple circuit scheme applied for testing the heat exchangers in steady
state conditions with TRACE

The fluid properties, as well as the flow properties obtained with TRACE are consistent
with the values expected from the preliminary calculation, providing a first code verifica-
tion. The power obtained from the simulation with TRACE and the outlet temperatures
of the salts should correspond to the imposed values in the MATLAB model (187.5 MW,
923 K for the primary salt, 943 K for the intermediate salt). Although a discrepancy
was observed and a smaller power was exchanged by the system. It was found that
the nodalization of the pipes and the heat structure has an impact on the results. A
cell length of 12 cm lowers the power exchanged with respect to the expected value by
approximately 5.4%; halving the cell length (6 cm, 20 cells) reduces the discrepancy to
2.7%. The causes are believed to be essentially numerical. A corse mesh enhances nu-
merical noise, which reduces the power exchanged. This effect is amplified through the
multiplication factor representing the total number of channels, of the order of 10^5.

The power and the outlet temperatures tend to the expected value from the preliminary
design with a finer nodalization, at the expense of computational time. The refining
of the nodalization was taken into consideration, but the maximal number of cells per
component in the primary circuit is limited. A subroutine of TRACE to model the
neutronics – fundamental for the simulation of the dynamics of the system in the transient
analysis (described in Sec. 2.4.1) – can handle maximally 20 cells per component, due

to memory constraints of the code. Another approach was followed to model correctly
the heat transfer. The total number of channels was artificially increased in order to
increase the heat transfer area. The augmentation in cross-sectional area of the heat
exchanger decreases the velocity (and the pressure drop) of the salts. Nevertheless the
Nusselt number is velocity independent, since the flow regime in the channels is laminar.
This implies that the heat transfer coefficient is not modified by an increase in the total
number of channels, but the overall heat transfer coefficient UA increases, due to an
increase in heat transfer area. The number of channels is increased until the exchange
power reaches 187.5 MW (1/16 of the nominal thermal power of the MSFR: 3000 MW).
This solution caused an increase in volume of salt by 0.02 m^3 (5.9%), which is negligible
in the frame of a preliminary assessment on the thermal hydraulics of the MSFR primary
and intermediate circuit.

2.2.1.2   Primary circuit

In order to simulate heat transfer in steady state and accidental conditions, the whole
primary circuit has to modeled. The proposed model takes into account the constraints
of the MSFR and constraints on flow properties (e.g. erosion).

The total volume of salt for the primary circuit of the MSFR was proposed to be 18 m^3
(as described in Sec. 1.4.1), with approximately half of it is allocated in the core. The
number of modules (out-of-core systems including heat exchanger, pump, off gas system
and the relative piping) is 16, resulting in a out-of-core volume of salt per module of
0.56 m^3.

The minimal flow area of the piping system (excluding core and heat exchanger) can be
obtained by dividing the volumetric flow rate $\dot{V} = \frac{\Gamma}{\rho}$ (defined by heat transfer constraint:
$\dot{Q} = \Gamma c_p \Delta T$) by the maximal allowed velocity in the pipes: 5 m/s (due to erosion). The
diameter of the pipes is therefore at minimum 29 cm. The volume of salt available for the
piping system can be obtained by subtracting the salt volume in the heat exchanger to
the out-of-core volume. Approximating the salt volume in the heat exchanger to 0.3 m^3
(see Sec. 1.4.1), the total length of the tubes is maximally 4 m. This value includes
the piping, the pumping system and the different plena needed as collector for the heat
exchanger.

The primary circuit is modeled in TRACE as follows. The total number of channels
of the heat exchanger is represented in TRACE by a pair of channels, multiplied by
the factor obtained by the previous simulation. The extremities of the heat exchanger
are connected to a *plenum* (inlet and outlet), which can be considered as the collectors
necessary to distribute the flow in the channels. In TRACE plena are components used

to connect pipes of different flow areas. A small volume of the plenum is chosen. The plenum placed at the inlet of the heat exchanger (hot leg) is designed to be the component responsible for the pressure control in the primary system by imposing a fixed pressure as a boundary condition. Two pipes, called *inlet* and *outlet* pipe relative to the heat exchanger, were placed between the heat exchanger and the *core*, with the help of two plena at each extremity of the pipes.

The core is modeled through a pipe with a fixed volume determined by the design of the MSFR where the primary salt heats up. Since the simulation regards only 1/16 of the circuit, the volume of salt in the core was downsized to this ratio: $V_{core} = 9/16 = 0.5625$ m^3. The length of the core-pipe was fixed by constraint to 3.5 m [6]. The flow area was calculated according to the length and the salt volume in the core.

TRACE allows the possibility of changing the orientation of the pipes. The heat exchanger is placed above the core to study natural circulation during accidents, therefore the two pipes (inlet and outlet) are orientated vertically.

A pump placed before the core in the cold leg is responsible for the fluid circulation. The pressure drops in the primary circuit are calculated using the expected flow properties and the pump head is estimated. In case of a pump trip, the pump becomes a momentum sink, therefore a pressure drop need to be modeled across the pump. The expected pressure drop in case of a pump trip is approximately 1 bar [7]. A friction factor f is added to the model such that the pressure drop across the pump at nominal velocity in case of loss of momentum source is 1 bar. The pump head is finally adapted to compensate this additional pressure loss in nominal operation conditions.

Heating of the primary salt occurs through a specific component of TRACE (*FLPOWER*) and a model developed for the simulation of delayed neutron precursors. Power is delivered directly to the fluid without a heat structure. For steady state conditions a total power of 187.5 MW is given to the salt mainly along the core, heating up the fluid from 923 K to 1023 K along the core. A more detailed description of the fluid heating modeling is given in Section 2.4.1. No additional heat losses were considered in the circuit.

A schematic view of the primary system can be seen on the bottom of Fig. 2.2, the dimensions of the pipes of the primary and intermediate circuit are listed in Tab. 2.1.

2.2.1.3   Intermediate heat exchanger

The heat removal system from the intermediate circuit is provided with an additional heat exchanger and a simple circuit with supercritical water considered as balance of plant. The latter is modeled with a constant mass flow rate and inlet temperature. Built-in
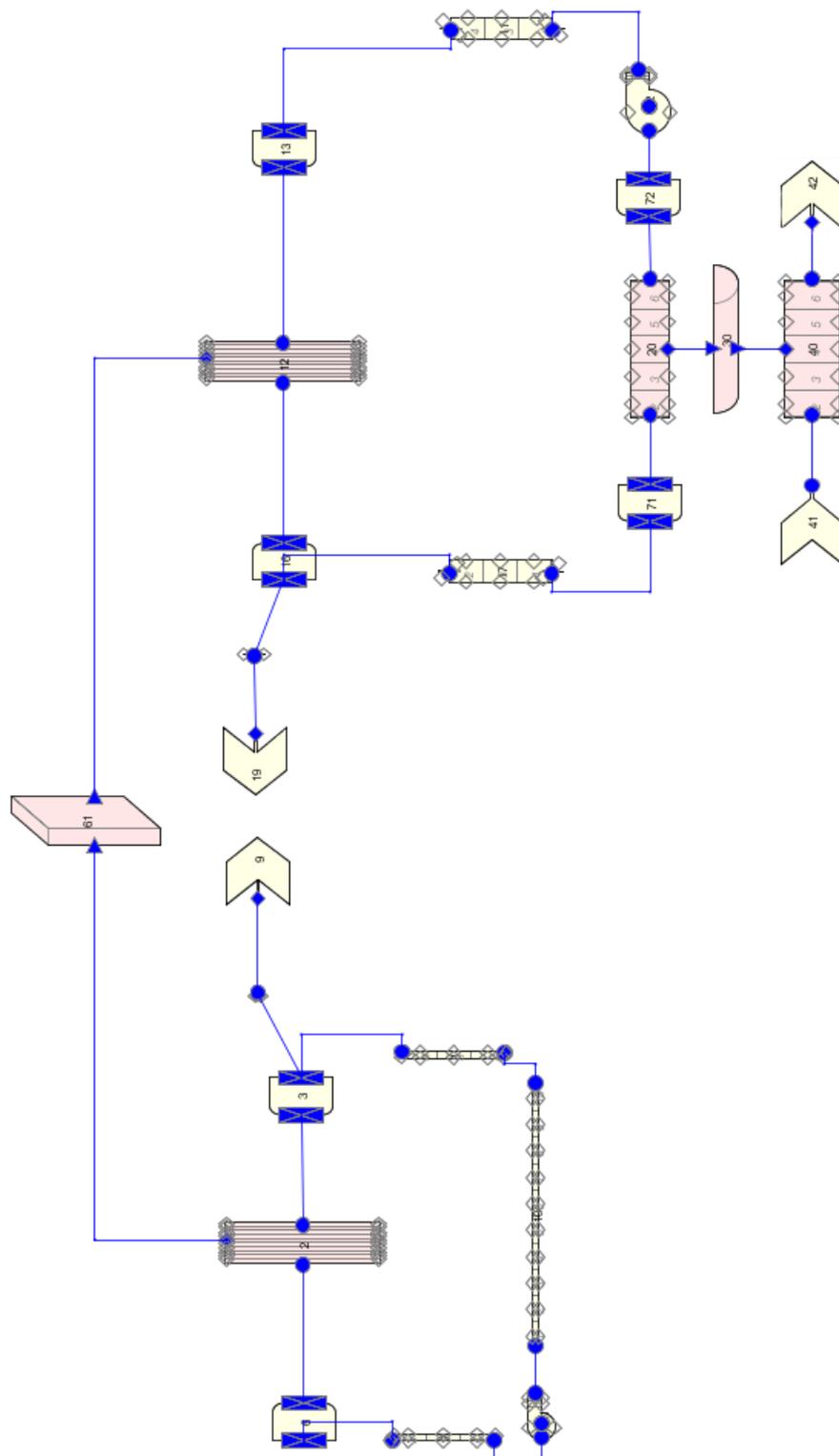
Figure 2.2. Modeled circuit with TRACE. The primary circuit can be seen in the bottom of the figure. The heat exchanger structure (left) connects the channels of the primary and intermediate system. The intermediate heat exchanger is shown on the top right and is connected to a simple circuit with supercritical water.

curve fits for the thermophysical properties of supercritical water are not implemented in TRACE, instead interpolation of steam tables are used. The interpolation scheme is based on the 1997 International Association for the Properties of Water and Steam (IAPWS) Industrial Formulation (IF97) standard [54].

A simulation with TRACE with fixed boundary conditions (flow rates and inlet temperatures) is performed to compare the results from the simulation with the expected values obtained from the MATLAB model. The heat transfer coefficient for the water side found with TRACE is higher by one order of magnitude than the expected coefficient obtained with the Gnielinski correlation. The thermal resistivity of the supercritical water is lower by a factor of 5 than the thermal resistivity of the salt. An underestimation of the heat transfer coefficient for the water side is therefore not affecting the overall heat transfer coefficient of the heat exchanger.

As for the case of the primary heat exchanger, the nodalization of the heat exchanger influences the heat transfer. A finer mesh (a cell length of 7 cm) decreased the error to +2%. In order to save computational time, the same approach used in the previous case was followed. The number of pipes was increased until the total exchanged power through the heat exchanger reached the desired value. The velocity in the channels and the Reynolds number decreases by increasing the cross-sectional area. The heat transfer coefficient of supercritical water consequently decreases, since the flow regime is turbulent. Again the impact on the overall HTC is negligible due to previous considerations.

2.2.1.4 Intermediate circuit

The intermediate circuit was designed similarly to the primary one. The size of the channels for primary heat exchanger is identical for both sides. Two plena are added to distribute the flow in the channels, and the pressure control component was added in the hot leg (at the outlet of the heat exchanger). The minimization of the intermediate salt volume is not a priority in this work, therefore no considerations are made in this sense. The salt volume in the heat exchanger is approximately 3 m^3 The maximal velocity in the inlet and outlet pipe is again fixed to 5 m/s. The expected flow rate obtained in the previous chapter allows to calculate the flow area and the hydraulic diameter of the inlet and outlet pipes. The height of the inlet and outlet pipe in the intermediate circuit is initially fixed arbitrarily to 4 m. A pump is added in the cold leg, following the same procedure described for the primary circuit above. The defined pressure drop (through a friction factor) across the pump right after a pump trip is 1 bar.

The dimensions of the pipes of the intermediate circuit are listed in Tab. 2.1. The
balance of plant is modeled by imposing the water flow rate, the inlet temperature and
the outlet pressure, fixed through the modeling of the heat exchanger (see Tab. 1.10).

TABLE 2.1. Dimensions of the modeled circuit

Primary circuit		
L inlet/outlet	[m]	1.30
D inlet/outlet	[m]	0.29
L core	[m]	3.50
D core	[m]	3.50
L pump	[m]	0.30
D pump	[m]	0.29
Secondary circuit		
L inlet/outlet	[m]	4.00
D inlet/outlet	[m]	0.38
L pump	[m]	0.30
D pump	[m]	0.38

2.3   Steady state analysis

The system is first analyzed in steady state conditions. The temperatures of the salts,
the velocities in different sections and the pressure drops across each component of the
system are compared with the expected values obtained from the preliminary analysis
(Tab. 2.2 and 2.3).

The results obtained from the steady state simulation agree well with the expected
results. Slightly different values (10% smaller) are found for the velocity in the power
generation circuit. The velocity of supercritical water was determined by the imposed
temperature difference across the intermediate heat exchanger and the required power
$\Gamma = \dot{Q}/(\Delta T c_p)$. During the design procedure of the intermediate heat exchanger, values
for density, thermal conductivity, heat capacity and viscosity were obtained from steam
tables at the expected average temperature. The large temperature variation influences
strongly the thermophysical properties and consequently the flow properties such as
velocity and pressure drop during the analysis with TRACE. Therefore the velocities in
the water circuit differs from the expected values, however the impact on the primary and
intermediate circuit is negligible due to previous considerations on the thermal resistivity
of the supercritical water.

Table 2.2. Results of TRACE simulation for steady state analysis with FliBe as intermediate salt for the primary and intermediate heat exchanger. Expected values are listed in square brackets.

Primary salt			
inlet temperature	[K]	1023.8	[1023.0]
outlet temperature	[K]	926.0	[923.0]
ΔT	[K]	97.8	[100.0]
average temperature	[K]	974.1	[973.0]
mass flow	[kg/s]	1401.5	[1383.8]
velocity in primary HX	[m/s]	1.1	[1.1]
velocity in core pipe	[m/s]	2.1	[2.1]
velocity in inlet pipe	[m/s]	5.1	[5.0]
primary HX pressure drop	[bar]	3.91	[3.83]
inlet pipe pressure drop	[bar]	0.53	[0.55]
outlet pipe pressure drop	[bar]	-0.47	[-0.50]
core pipe pressure drop	[bar]	0.01	[0.01]
total pressure drop	[bar]	3.97	[3.90]
Intermediate salt			
inlet temperature	[K]	862.1	[863.0]
outlet temperature	[K]	946.8	[943.0]
ΔT	[K]	84.77	[80.0]
mass flow	[kg/s]	941.3	[980.7]
velocity in primary HX	[m/s]	1.8	[1.9]
velocity in intermediate HX	[m/s]	0.6	[0.6]
velocity in inlet pipe	[m/s]	4.7	[5.0]
primary HX pressure drop	[bar]	4.52	[4.8]
inlet pipe pressure drop	[bar]	-0.62	[-0.64]
outlet pipe pressure drop	[bar]	0.66	[0.70]
intermediate HX pressure drop	[bar]	0.39	[0.42]
total pressure drop	[bar]	4.96	[5.29]
ΔT$_{LM}$ HX	[K]	70.67	[69.5]
Supercritical water			
inlet temperature	[K]	800.0	[800.0]
outlet temperature	[K]	913.9	[913.0]
ΔT	[K]	113.9	[113.0]
mass flow	[kg/s]	568.2	[568.2]
velocity in intermediate HX	[m/s]	9.3	[8.7]

TABLE 2.3. Results of TRACE simulation for steady state analysis with FliNaK as intermediate salt for the primary and intermediate heat exchanger. Expected values are listed in square brackets.

Primary salt			
inlet temperature	[K]	1023.5	[1023.0]
outlet temperature	[K]	925.5	[923.0]
ΔT	[K]	98.0	[100.0]
average temperature	[K]	974.5	[973.0]
mass flow	[kg/s]	1397.0	[1383.8]
velocity in primary HX	[m/s]	1.0	[1.0]
velocity in core pipe	[m/s]	2.1	[2.1]
velocity in inlet pipe	[m/s]	5.1	[5.0]
primary HX pressure drop	[bar]	3.56	[3.48]
inlet pipe pressure drop	[bar]	0.53	[0.55]
outlet pipe pressure drop	[bar]	-0.47	[-0.50]
core pipe pressure drop	[bar]	0.01	[0.01]
total pressure drop	[bar]	3.63	[3.54]
Intermediate salt			
inlet temperature	[K]	866.8	[863.0]
outlet temperature	[K]	945.9	[943.0]
ΔT	[K]	79.1	[80.0]
mass flow	[kg/s]	1261.0	[1246.7]
velocity in primary HX	[m/s]	1.8	[1.7]
velocity in intermediate HX	[m/s]	0.6	[0.6]
velocity in inlet pipe	[m/s]	5.0	[5.0]
primary HX pressure drop	[bar]	2.11	[2.23]
inlet pipe pressure drop	[bar]	-0.73	[-0.77]
outlet pipe pressure drop	[bar]	0.77	[0.82]
intermediate HX pressure drop	[bar]	0.20	[0.20]
total pressure drop	[bar]	2.34	[2.48]
ΔT LM	[K]	67.7	[69.5]
Supercritical water			
inlet temperature	[K]	800.0	[800.0]
outlet temperature	[K]	907.2	[908.0]
ΔT	[K]	107.2	[108.0]
mass flow	[kg/s]	568.2	[568.2]
velocity in intermediate HX	[m/s]	7.1	[8.0]

2.4   Transient analysis

The aim of this section is to analyze the performance of the primary heat exchanger in case of accident. The heat exchanger is coupled to the primary and intermediate circuit, and indirectly to the ultimate heat sink, represented by the supercritical water circuit. The performance of the heat exchanger must be therefore analyzed in the frame of the global system. The considered transient is a station black out (SBO), which features a trip of primary and intermediate circuit pump, a reduction of flow rate in power cycle circuit and no SCRAM simulated.

The *final* steady state after the transient was compared to the *nominal* steady state. The temperatures of the salts and heat structure, as well as the power generated in the primary circuit are the most concerned parameters. The capability of the heat exchanger to withstand accidental conditions will be assessed by comparing the values obtained by the simulation (in particular temperatures) to the physical and technological limits of the salts and the structural material.

The set up of natural circulation (NC) in case of a pump trip is crucial to avoid to exceed the temperature boundaries of the salt and structural material. The primary heat exchanger was therefore placed at different heights relative to the core pipe and the results were compared.

An analysis on the ultimate heat sink was conducted in the frame of a SBO transient. The flow rate of supercritical water was reduced during the transient and the response of the system was investigated. A minimal flow rate was obtained such that the system reaches an equilibrium, without compromising the structural material of the circuits.

Different intermediate salts were investigated starting from the same conditions (heat exchanger height and water flow rate) and the final steady states of the system were compared.

2.4.1   Modeling parameters

Pump trip

The decrease in flow rate has to be modeled in case of a pump trip. For the MSFR a time constant τ of 10 s of the pump coast down is assumed, which represents a pump with a medium size flywheel [7]. The pump trip is simulated using the built-in component *trip* in TRACE. The moment of inertia of the pump is tuned such that the initial exponential decrease of the flow rate ($e^{-t/\tau}$) fitted the desired curve at the beginning of the transient.

Neutronics modeling

The power generated in a reactor is governed by neutron kinetics. The doppler effect in
the fuel, the fuel expansion effect, the delayed neutron precursors (dnp) and the neutron
generation time are the main responsible parameters of the free dynamics of the system.
The power of a MSR is therefore determined by these parameters, unless user controlled
reactivity (external reactivity) is inserted into the system. In a MSR the decay heat is
distributed along the whole primary circuit through the presence of fission products.

A delayed neutron precursors transport model for TRACE was developed by
Matteo Zanetti in the frame of a collaboration between PSI and Politecnico di Milano
(POLIMI). The neutron kinetics was implemented using a 0-D model, the precursors
transport features a 1-D model.

The distribution of dnp (divided in eight groups) in the primary circuit is computed
according to the parameters of the system: nominal power, prompt neutron lifetime,
decay constants of each dnp group, fluid velocities and volumes of the components. Once
the concentration of dnp reached an equilibrium state, the power computation module
can be activated. A user defined fraction of the nominal power (called *decay power*)
produced in the core is distributed through the primary circuit. A decay constant for
the decay heat is set by the user.

During steady state the total power delivered to the fluid is constant, but the distribution
changes slightly after the activation of the dnp model. In case of a transient such as a
pump trip the flow properties change as well as the temperatures. The flow properties
modify the dnp concentration while the feedback acts on the in-core delivered power.

Decay heat

A detailed analysis of the decay heat for a MSR is a complex task and is beyond the
scope of this thesis. The aim of this brief section is to describe the modeling of the decay
heat used for the analysis with TRACE and its impact on the behavior of the system.

In a MSR fission products are not confined to the core, but circulate through the primary
circuit with the salt. The heat produced by the decaying fission products is distributed
along the primary circuit, according to the salt volumes. In case of a loss-of-flow accident
in the primary circuit the distributed decay heat has a negative impact on the natural
circulation: the difference in density driving NC is slightly decreased with respect to
a system where the heat source is placed on the bottom of the circuit, since the fluid
is heated also on the upper part. Therefore an accurate modeling of the decay heat is
necessary to simulate the primary circuit of the MSR.

The dnp transport model simulates the decay heat using two parameters set by the user: the fraction of the total power corresponding to the decay power and its decay constant. The power fraction is distributed in the primary circuit according to the salt volumes, allowing the fluid to heat up outside the core. In case of a decrease in the prompt power (e.g. transient) the decay power decreases exponentially (with the decay constant set by the user) until the fraction of the new equilibrium power is reached, stabilizing the power on a new state.

Three groups of decay constants were proposed for the MSFR, each with a different power share [3] (listed in Tab. 2.4). Figure 2.3 shows the evolution of the total decay power with time, obtained by summation of the functions of the three decay groups. In the dnp model a single decay constant and power fraction can be set. The fraction of power considered as decay power is obtained by summing the three power share values (4.32%). A conservative decay constant was chosen (listed in Tab. 2.4) to model the decay power evolution, such that the decay heat function $4.32\%e^{-\lambda t}$ implemented in TRACE always overestimates the decay power evolution proposed in [3]. The consequences are described in the next paragraph.

In this thesis work the neutronic of the system depends only on thermal hydraulic properties since no SCRAM is modeled (unprotected accidental conditions are investigated). The total power produced is composed by the prompt power and the fraction considered as decay power. In case of a loss-of-flow accident the prompt power produced in the circuit decreases suddenly (an exhaustive analysis is provided in Section 2.4.2) but the decay heat mitigates the total power drop. A smaller decay constant induces the decay power contribution to the total power to last longer, but the achieved equilibrium state after the transient – where the decay power fraction is 4.32% of the total power – is not influenced by the decay heat constant. Therefore a conservative choice for the decay constant is not affecting the investigate final steady state.

TABLE 2.4. Decay heat constants and power fractions for modeling decay heat with three groups. The last line lists the chosen value for the decay constant and power fraction used in TRACE [3].

| Decay heat group	λ_i [1/s]	Power fraction [%]
1	0.1973	1.17
2	0.0168	1.29
3	3.58E-4	1.86
TRACE	3.70E-4	4.32
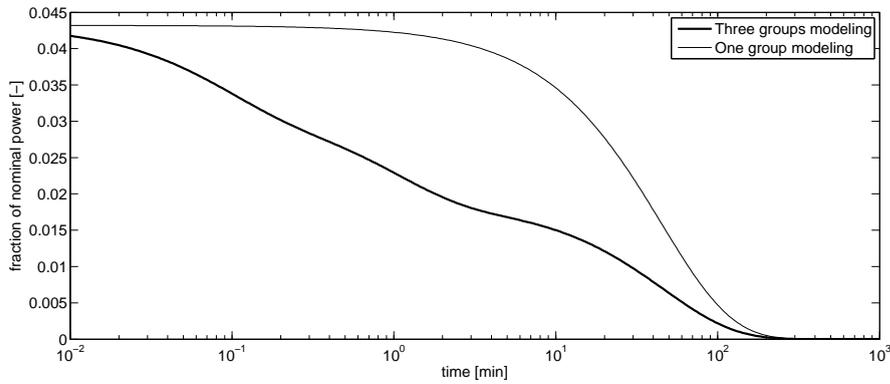
FIGURE 2.3. Decay power evolution with time modeled with three groups and with
one group

2.4.2   Results

2.4.2.1   Reactivity variation due to a change in dnp concentration

Delayed neutron precursors in circulating-fuel reactors are mainly produced in the core
and are transported with the primary salt. Depending on their decay constant and on
the salt in-core and out-of-core residence time, the emission of a neutron can take place
out of the core [9]. In nominal operation the reactor is in equilibrium and the reactivity
loss due to circulating dnp is balanced. A change of flow rate in the primary circuit
modifies the distribution of the dnp, acting therefore on the reactivity of the system.

An analytical analysis [3] is conducted to have a first insight of the above described
dnp model. For the modeled circuit the primary flow rate is changed and the effects on
reactivity and temperature are analyzed. Analytical results are compared to the findings
from TRACE simulation obtained with the dnp model.

The equation governing the variation of reactivity between the *initial* and *final* steady
state after a transient of a reactor is

$$\delta\rho = (\alpha_d + \alpha_D)\delta T_{\mathrm{AV}} + \delta\rho_0 + \delta\rho_{\mathrm{ext}} = 0. \tag{2.1}$$

$(\alpha_d + \alpha_D)\delta T_{\mathrm{AV}}$ indicates the reactivity variation due to a variation of the average core
temperature. $(\alpha_d + \alpha_D)$ is the fuel feedback coefficient, α_d is the fuel expansion coefficient
while α_D is the Doppler feedback coefficient. $\delta\rho_0$ is the reactivity variation due to a
variation in velocity and ensuing out-of-core decay of delayed neutron precursors [3].

In case of a transient with no external reactivity insertion, the change in the average temperature of the core depends only on the reactivity change due to the dnp

$$(\alpha_d + \alpha_D)\delta T_{\text{AV}} = -\delta\rho_0. \tag{2.2}$$

The reactivity contribution (0-D model) from the dnp can be expressed [3] as

$$\rho_0 = \sum_{i=1}^{8} \frac{\beta_{\text{eff}}^i \lambda_i}{\lambda_i + \frac{1-e^{-\lambda_i \tau_{\text{EC}}}}{\tau_{\text{C}}}}, \tag{2.3}$$

where i represents the group of precursors, β_{eff}^i is the fraction of dnp for each group, λ_i the decay constant of dnp group i, τ_{EC} is the out-of-core transit time and τ_{C} is the core transit time.

The equilibrium kinetic parameters used for this calculation are taken from [3] and are listed in Tab. 2.5.

TABLE 2.5. Equilibrium kinetics safety parameters (8 groups) of the MSFR [3].

		λ [1/s]	β_{eff} [pcm]
g^1		1.25E-02	22.8
g^2		2.83E-02	50.0
g^3		4.25E-02	41.6
g^4		1.33E-01	66.7
g^5		2.92E-01	106.5
g^6		6.66E-01	18.5
g^7		1.63	23.4
g^8		3.55	5.3
Total			334.8
neutron generation time	[μs]		0.95
Doppler coeff	[pcm/K]		-3.25
Fuel exp coeff	[pcm/K]		-3.01
Fuel coeff	[pcm/K]		-6.26

A change in flow rate modifies the reactivity contribution from the delayed neutron precursors and according to Eq. 2.2 a change in the core average temperature is expected. No other parameters can modify the core average temperature of the system.

Two simulations with a pump trip are conducted with TRACE. For both cases the primary and intermediate circuit pump are tripped; different flow rates (1.1% and 1.6% of the nominal flow rate) in the primary circuit at the end of the transient are set up. The velocities obtained from the output of TRACE are used to calculated the in-core and out-of-core residence time (using the dimensions of the pipes in Tab. 2.1), presented in Tab. 2.6. The change in reactivity and the increase in core average temperature are

calculated with Eq. 2.2. The increase in core average temperature is obtained also from TRACE.

Tab. 2.7 presents the results obtained with the analytical approach as well as the results from the simulations.

TABLE 2.6. Velocities in the primary circuit in case of a reduction in flow rate to 1.1% and 1.6% of the nominal flow rate.

Mass flow rate fraction	[-]	100%	1.1%	1.6%
velocity HX	[m/s]	1.01	0.01	0.02
velocity inlet pipe	[m/s]	5.05	0.06	0.09
velocity outlet pipe	[m/s]	4.95	0.06	0.08
velocity core	[m/s]	2.08	0.02	0.03
velocity pump	[m/s]	4.95	0.06	0.08
τ_{EC}	[s]	1.7	151.5	101.1
τ_C	[s]	1.7	146.4	104.8

TABLE 2.7. The variation of the reactivity as well as the difference of the core average temperature with respect to the nominal flow rate. A comparison with the results obtained with TRACE is shown.

Mass flow rate fraction	[-]	1.1%	1.6%
$\Delta\rho_0$	[pcm]	122	114
ΔT	[K]	20	18
ΔT TRACE	[K]	35	34

The core average temperature increase obtained with TRACE is larger by 70% than the value expected from the analysis with the 0-D model. Different possible causes were investigated. The 0-D model considers a constant concentration of delayed neutron precursors over the core region. In a circulating-fuel reactor (and in the dnp model used in TRACE) the distribution of dnp depends on the generation and decay of dnp in a moving system. A higher concentration of dnp is expected towards the core outlet, since the dnp are produced along the core and the decay constants are small enough to avoid a complete decay in the core. This approximation underestimates the precursor loss by 10% [11], therefore it can not be the main reason for the discrepancy. Numerical reasons in the dnp solver are believed to be the cause for the different final core average temperature (private communication with Matteo Zanetti).

The average core temperature increase obtained with TRACE is 35 K, for a final flow rate in the primary circuit of 1.1% of the nominal value. During loss-of-flow accidents the relevant parameters are the temperatures in the hot and cold leg of the system. In the first case it should be limited in order to avoid high creep rates in structural materials, while the temperature in the cold leg should be high enough not to reach the freezing point. The difference in temperature between the hot and cold leg is expected to reach

several hundreds of K in case of a station black out accident. An underestimation of
few degrees in the core average temperature is therefore not significantly affecting the
behavior of the system for a preliminary analysis,

2.4.2.2   General observations and phenomenological description

The behavior of the system designed with FliBe as intermediate salt during a SBO
accident is first investigated. A comparison of the systems with different secondary salts
is given in the last section.

The power generated in the primary circuit is limited by the effects of neutronics and by
the heat balance equation

$$\dot{Q} = \Gamma c_p \Delta T \tag{2.4}$$

The minimal and maximal temperatures at the inlet and outlet of the core in the primary
circuit can not reach arbitrary values. The minimal temperature is the water inlet
temperature 800 K. For estimation purposes the core average temperature (fixed by the
neutronics) is assumed to be constant (973 K). Therefore the maximal temperature
difference can be estimated to 346 K, while the nominal value is 100 K. Equation 2.4
states that the maximal power produced in the primary system is

$$\frac{\dot{Q}}{\dot{Q}_0} = \frac{\Delta T}{\Delta T_0} \frac{\Gamma c_p}{\Gamma_0 c_{p,0}} = 3.46 \frac{\Gamma c_p}{\Gamma_0 c_{p,0}}.$$

Assuming the final salt flow rate to be 1% of the nominal value and a constant heat
capacity (which is the case for the primary salt), the new power generated in the circuit
is maximal 3.46% of the nominal power.

The influence of the water circuit on the system is now investigated. During nominal
operation the water flow rate is kept constant, but needs to be adapted in view of a
SBO accident. The balance of plant is modeled with Fill-Break components, therefore a
pump trip can not be included into the model. The flow rate of the water circuit must be
defined manually, therefore in case of a SBO accident a decrease in flow rate and a final
value need to be modeled. The final steady state after the transient is the focal point
of the analysis. The water flow rate is reduced in short time after the pump trip to its
final value. Two values for the water flow rate at the end of the transient are simulated:
1% and 5% of the initial steady state flow rate. The primary and intermediate pumps
are tripped and no external reactivity is inserted, leaving the free dynamics to achieve a
new equilibrium state.

The temperature evolution at the inlet and outlet of the heat exchanger, as well as the
core average temperature (Fig. 2.4) are the first investigated parameters.
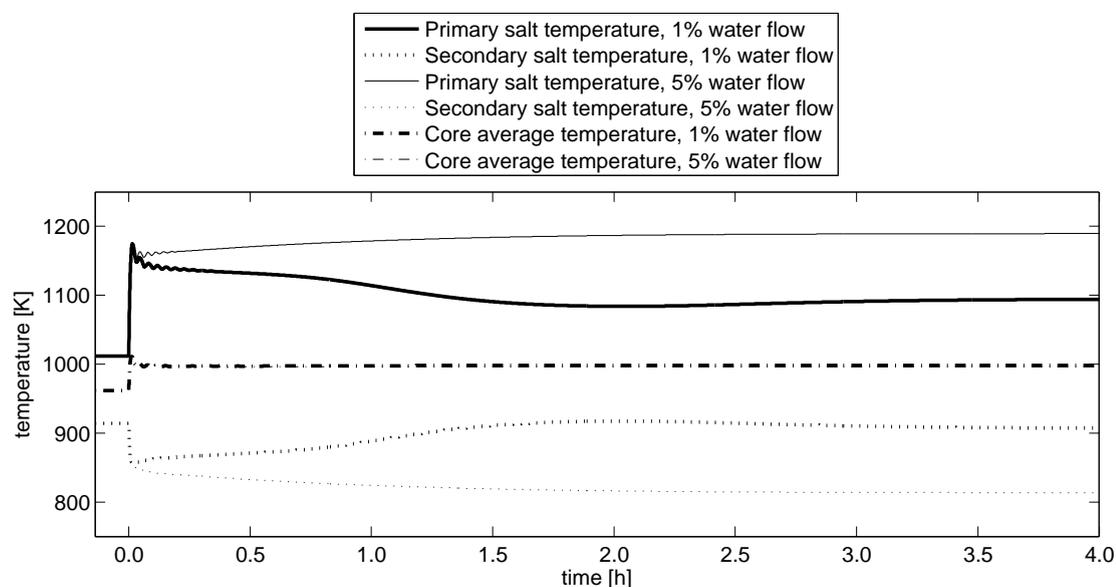
FIGURE 2.4. Inlet and outlet temperatures evolution after a primary and intermediate
pump trip (time 0) of the primary salt in the primary heat exchanger. No external
reactivity was inserted. Value for two different water flow rates are shown. The core
average temperature is described by the dashed line.

The core average temperature increases by a similar amount for the case with 1% and
5% water flow rate (numerical values are listed in Tab. 2.7). The small differences are
caused by a slight different primary salt flow rate obtained through natural circulation
(1.1% of the nominal value for the 1% water flow rate case, 1.6% for the 5% water flow
rate), which determines the residence time of the salt in the core and out-of-core region.

A stronger NC is caused by a larger density difference between the hot and the cold leg
of the primary system, in fact the maximal temperature at the end of the transient is
obtained for a higher water flow rate. Since the core average temperature is fixed through
the neutronics, the minimal temperature in the cold leg is obtained for a higher water
flow rate. Numerical values of the flow rates, power and temperature in initial and final
steady state for the two different cases are listed in Tab. 2.8.

The power evolution for the two final water flow rates is shown in Fig. 2.5. A higher
power (which is the cause for a higher temperature in the cold leg and a stronger natural
circulation) is found for the case where water flows at a higher rate. The description
of the phenomena leading to a higher power produced for a higher water flow rate is
postponed after the analysis on the temperature distribution in the heat exchanger.

The temperature distribution of the fluids across both heat exchangers is determined by
the salt flow rates and the water flow rate. Figures 2.6a and 2.6c present the temperature
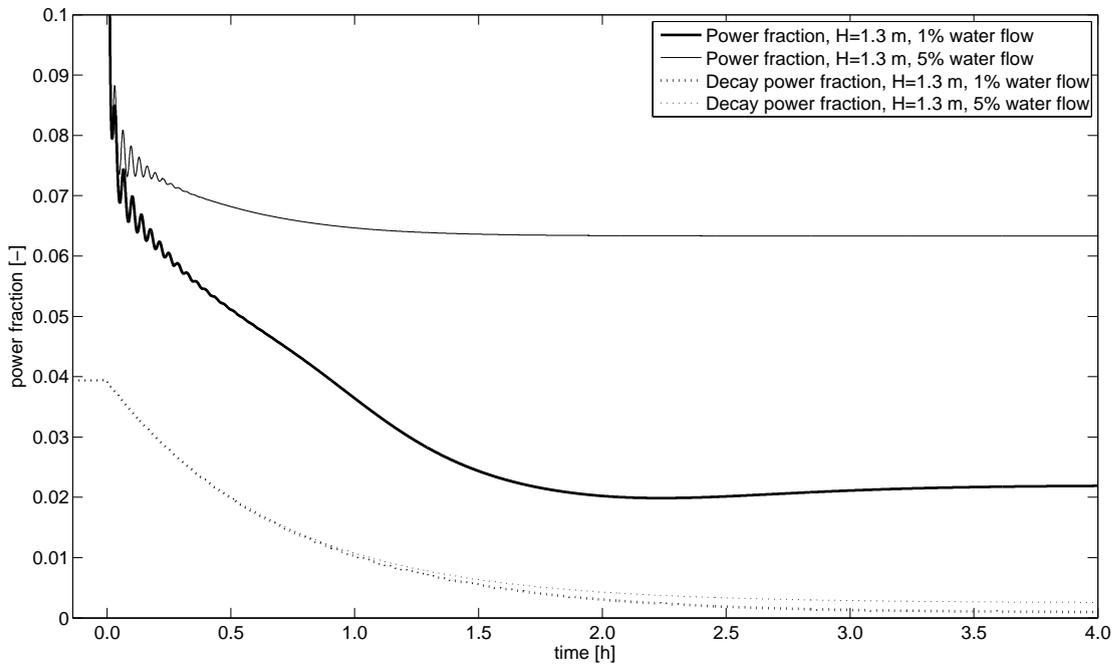
FIGURE 2.5. Normalized power evolution after a pump trip in primary and intermediate
circuit. The power evolution is plotted for two water flow rates. The fraction of the
power representing decay heat is presented with the dotted lines.

TABLE 2.8. Steady state conditions results after a SBO transient. Two final water flow
rates and two different heights between core and primary heat exchanger are simulated.
Values for flow rates are normalized to nominal steady state conditions.

		nominal	1% water flow		5% water flow	
Primary HX height	[m]		1.3	4.0	1.3	4.0
power $\dot{Q}$	[-]	-	2.19%	2.24%	6.33%	7.03%
primary salt flow rate Γ_1	[-]	-	1.14%	1.68%	1.64%	2.75%
intermediate salt flow rate Γ_2	[-]	-	1.20%	1.20%	1.74%	1.87%
ΔT primary salt	[K]	97.1	187.8	131.6	376.3	251.3
ΔT avg core	[K]	-	37.2	35.2	35.4	32.0
ΔT intermediate salt	[K]	82.2	151.9	154.4	302.3	311.4
ΔT water	[K]	105.8	252.2	257.2	138.5	155.1

distribution of the primary and intermediate salt along the primary heat exchanger for
the two different water flow rates. In Figs. 2.6b and 2.6d the temperature distribution
of the intermediate salt and water along the intermediate heat exchanger is shown. The
primary salt cools down from left to right, the intermediate salt heats up from right
to left (counterflow arrangement). The area between the primary and intermediate salt
curves expresses the exchanged power, in fact $\dot{Q} = \int \frac{UA}{L} \Delta T(x) dx$.

In nominal conditions the lines are parallel and the heat flux is constant along the heat
exchanger. In case the flow rates deviate from their nominal values, the temperature
distribution curve of one salt tends to flattens on the other. The parameter describing

which curve tends to approach the other is the ratio of $\Gamma_i c_{p,i}$

$$r_i = \frac{\Gamma_h c_{p,h}}{\Gamma_c c_{p,c}} / r_{\text{nom}} \quad i = 1, 2 \tag{2.5}$$

where h stands for hot fluid, c for cold fluid and $r_{\text{nom}} = \frac{(\Gamma_h c_{p,h})_0}{(\Gamma_c c_{p,c})_0}$ is the ratio in nominal conditions (to normalize r), 1 represents the primary heat exchanger, 2 the intermediate.

The volumetric heat capacity ρc_p describes the ability of a given volume of a substance to store internal energy while undergoing a given temperature change[1]. This quantity can be applied to a dynamic system by multiplying it with a volumetric flow rate $\dot{V}$, obtaining Γc_p, which measures the increase in temperature of a stream subject to a heat source ("thermal inertia of a flow").

The effect of the ratio r is evident when comparing Figs. 2.6b and 2.6d. In the first case the temperature distribution of water (cold fluid) flattens on the curve of the salt because the water flow rate is low ($r_2 \gg 1$). In the second case, where the water flow rate increased by 5 times, the opposite is observed: the hot salt cools down until the water inlet temperature is reached ($r \ll 1$).

The power difference in case of different in water flow rates can be described with the help of the parameter r. The high water flow rate ($r_2 \ll 1$) determines a very low intermediate salt outlet temperature (800 K) from the intermediate heat exchanger. The temperature distribution in the primary heat exchanger tends again to the cold fluid (intermediate salt), in fact $r_1 = 0.95$. The outlet temperature of the primary salt tends to be low, while the core average temperature is fixed by neutronics. Therefore the temperature of the primary salt in the hot leg (at the outlet of the core) is high. A high temperature difference between the inlet and outlet of the heat exchanger in the primary circuit determines a high produced power (6.33% of the nominal power), since the balance between the power produced in the core and the power exchanged in each heat exchanger must be respected in steady state.

In case $r_2 \gg 1$ (Fig. 2.6b) the intermediate salt outlet temperature does not tend to a low value in the intermediate heat exchanger. Therefore the primary salt is not cooled as in the previous case and the power produced in the core is lower (2.19% of the nominal power). In this case $r_1 = 0.94$.

A change in flow rates of the salt does not affect the overall heat transfer coefficient of both heat exchangers since the Nusselt number is virtually constant (due to the laminar flow regime). The thermal resistance of supercritical water is negligible compared to

---

[1]http://en.wikipedia.org/wiki/Volumetric_heat_capacity
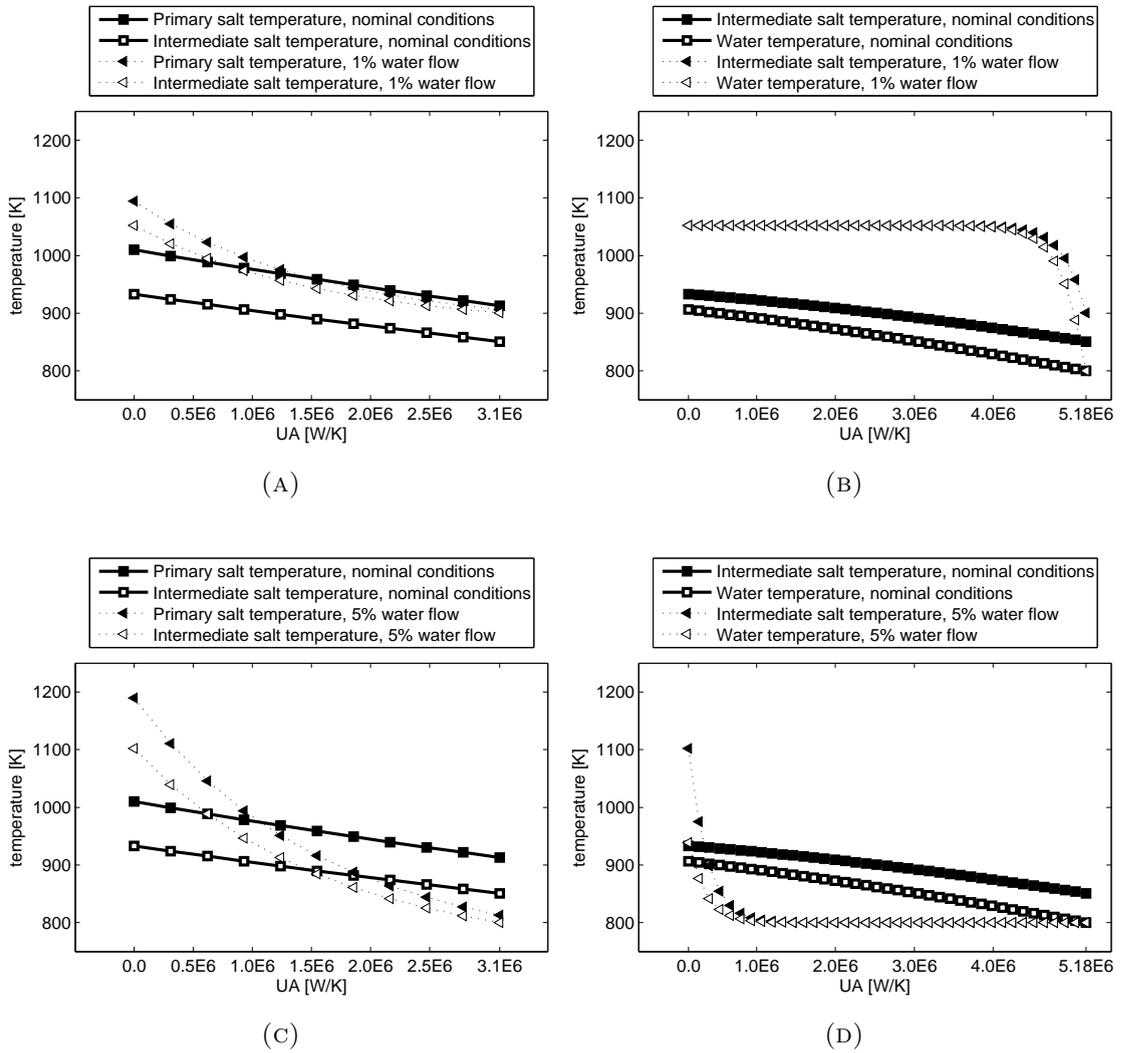
FIGURE 2.6. Temperature distribution along the primary heat exchanger (left) and
intermediate heat exchanger (right). The nominal case, the 1% and the 5% water flow
rate case are shown.

the resistance of the salt, therefore a variation in the water flow rate does not change
significantly the overall heat transfer coefficient of the intermediate HX.

The power exchanged by both heat exchangers could theoretically be calculated from
Eq. 1.1, using the constant overall heat transfer coefficient and the logarithmic mean
temperature difference (Eq. 1.3). This is not possible anymore in the cases after the
transients: the temperatures at one side of the heat exchanger are very similar, therefore
the logarithmic mean temperature difference becomes very sensitive to small variations in
temperature. Numeric tolerance of TRACE of few degrees has virtually no influence on
the behavior of the system, but heavily affects ΔT_{LM} and therefore the power exchanged
calculated with this method. It is therefore not suitable to calculate the power exchanged
via Eq. 1.1.

2.4.2.3   Influence of natural circulation on system behavior

Core - Primary HX   A second set of simulations are conducted with a different relative height of the heat exchanger with respect to the core. The inlet and outlet pipes are stretched to 4 m, while maintaining the same flow area (to keep the same salt velocity). Table 2.8 lists the flow rates in primary and intermediate circuit, for 1% and 5% water flow rate, for H=1.3 m and H=4.0 m. The temperature distribution along primary and intermediate heat exchanger are compared for the case $H = 1.3$ m and $H = 4$ m in Figs. 2.7a and 2.7b.

In Fig. 2.7 it can be seen that the curvature of the temperature distribution along the primary heat exchanger changes from concave to convex. The ratio r_1 becomes positive. The behavior of the system depends on the flow rate of the water circuit, therefore on r_2:

- $r_2>1$ (1% water flow rate), the temperature difference of the intermediate salt between the inlet and outlet of the intermediate HX is limited (the salt does not cool down excessively), as for the case with $H = 1.3$ m. The natural circulation is improved in the primary circuit and $r_1 > 1$. The power increased slightly with respect to the case with $H = 1.3$ m, but the temperature difference between hot and cold leg in the primary circuit decreased by 30%, which is favorable in case of accident.

- $r_2<1$ (5% water flow rate), the intermediate salt cools down reaching very low values (approximately 800 K). The intermediate cold salt flows through the primary heat exchanger and cools the primary salt, but due to the improved natural circulation in the primary circuit ($r_1 > 1$) the increase in primary salt temperature is lower (more than 30%). The power produced in the core is higher (7.03% compared to 6.33% of the nominal power) than for the case $H = 1.3$ m, nevertheless from a safety point of view the relevant parameter are the temperatures, which tend to a safer state

Primary HX - Intermediate HX   The height difference between the primary and intermediate heat exchanger is doubled, reaching 8 m. The effects of improving the natural circulation in the intermediate circuit on the safety of the system is investigated. The temperature distribution along primary and intermediate heat exchanger are compared for the case $H = 4$ m and $H = 8$ m in Figs. 2.7c and 2.7d.

The normalized flow rate of the intermediate salt increases from 1.20% to 1.46%. In terms of Γc_p ratio a decrease is observed (from 0.95 to 0.75) which flattens the curve of
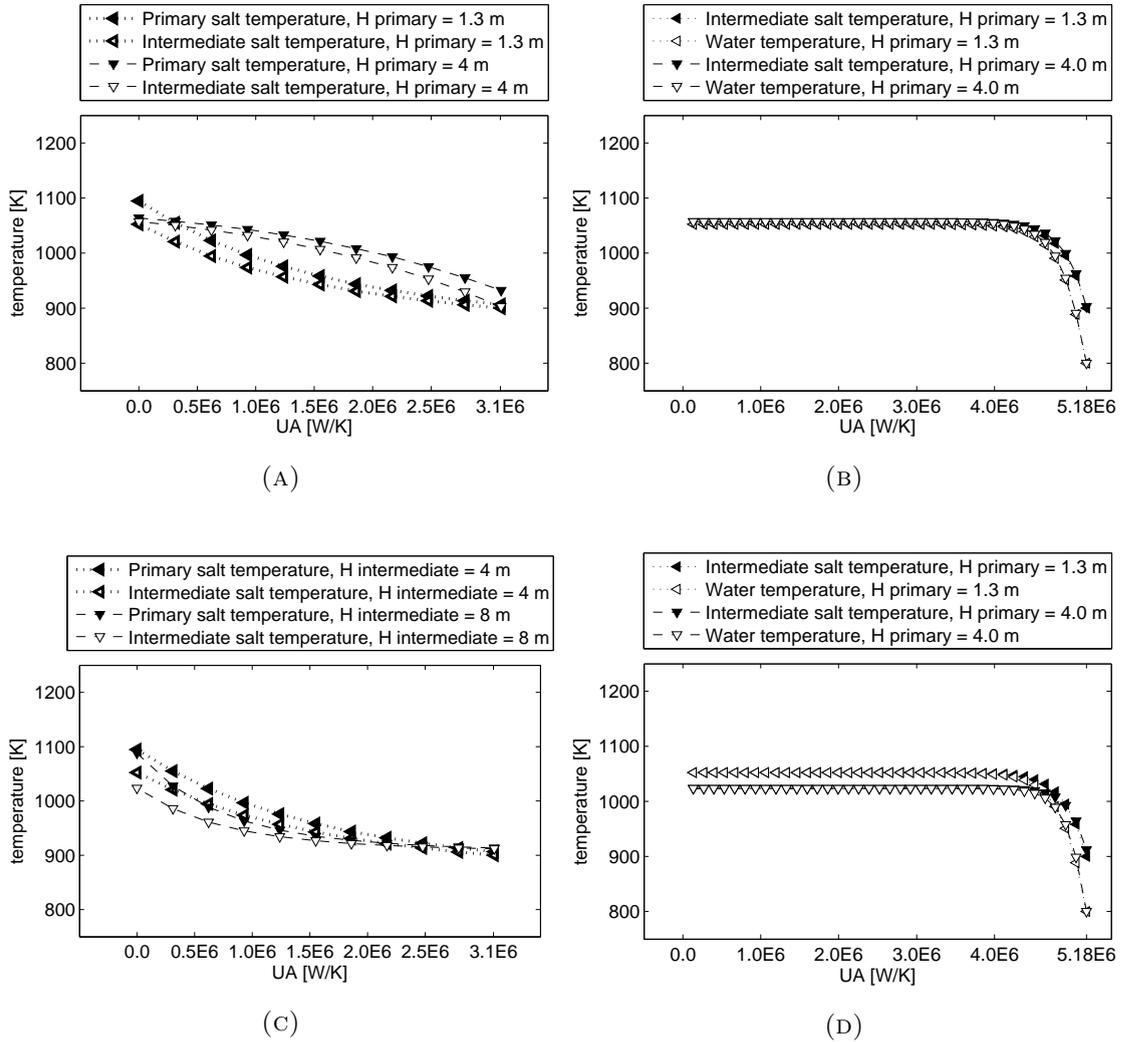
FIGURE 2.7. Temperature distribution along the primary heat exchanger (left) and intermediate heat exchanger (right). Curves for two height differences between core and HX (top), curves for two height differences between primary HX and intermediate HX (bottom) are shown. The water flow rate is set at 1% of the nominal value.

the primary salt on the intermediates salt, while keeping the temperatures in the hot and cold leg of the primary circuit almost constant to the case $H = 4$ m (a decrease of 13 K, corresponding to 8%)

The power exchanged in the primary heat exchanger (see Fig. 2.7c) is almost confined towards the inlet nozzle of the primary salt, while towards the outlet no temperature difference can be observed between the primary and intermediate salt, therefore the heat flux is virtually zero. Besides this, from Fig. 2.7c it can be recognized that the area between the two curves representing primary and intermediate salt is lower for the $H = 8$ m than $H = 4$ m case. The area represents the power exchanged and – since the heat balance must be respected – the power produced in the core. In fact a decrease in

power is observed (10% less, which corresponds to (0.4 MW).

The results for two height differences between primary and intermediate heat exchanger
are summarized in Tab. 2.9.

TABLE 2.9. Effect of natural circulation improvement on the intermediate circuit on
the steady state conditions at the end of a SBO accident.

Intermediate HX height	[m]	4.0	8.0
power $\dot{Q}$	[-]	2.19%	1.96%
primary salt flow rate Γ_1	[-]	1.14%	1.10%
intermediate salt flow rate Γ_2	[-]	1.20%	1.46%
ΔT primary salt	[K]	187.8	174.1
ΔT avg core	[K]	37.5	37.4
ΔT intermediate salt	[K]	151.9	111.73
ΔT water	[K]	252.2	223.5

2.4.2.4   Comparison between two different salts

Two different intermediate salts have been investigated: FliBe and FliNaK. The heat ex-
changer designed using the properties of FliNaK (see Tab. 1.9) was modeled in TRACE
following the same procedure as for the case with FliBe. The primary circuit was not
modified while changing from the configuration with FliBe to FliNaK, since the primary
salt volume requirements for the heat exchanger are similar. The height difference be-
tween the core and primary heat exchanger is kept at 1.3 m. The height between primary
and intermediate heat exchanger is 4 m for both configurations.

The thermal expansion coefficient changes the density of the salt between the heat source
(bottom) and the heat sink (top), which drives natural circulation. FliNaK salt has a
higher expansion coefficient (0.642 kg/m^3·K than FliBe (0.488 kg/m^3·K), therefore for
the same temperature difference between hot and cold leg in the intermediate circuit the
natural circulation for FliNaK is enhanced with respect to FliBe. Table 2.10 presents
the results for the final steady state after a SBO accident. As expected from the thermal
expansion coefficients the normalized flow rate for the intermediate salt is higher for the
configuration with FliNaK.

The effects of a stronger NC in the intermediate circuit are similar as those described
in Tab. 2.9 for an enhanced NC due to an increased height difference between primary
and intermediate heat exchanger. The power produced in the primary circuit is lower
for the FliNaK case, due to an increase of the value r_2. A large r_2 value avoids a low
outlet temperature of the intermediate salt form the intermediate heat exchanger, which
would lead to higher power production. The temperature difference of the intermediate

salt between inlet and outlet of the (intermediate) heat exchanger decreases, which is positive from a safety point of view.

The smaller increase in core average temperature is a consequence of the different design of the heat exchanger (velocities and channel length in the HX). This aspect is less relevant since the increase in core average temperature is negligible with respect to a temperature difference of hundreds of K across the heat exchanger (respectively the core).

TABLE 2.10. Effect of two different intermediate salts on the final steady state after a SBO transient

Intermediate salt		FliBe		FliNaK	
		nominal	SBO	nominal	SBO
power $\dot{Q}$	[-]	-	2.19%	-	2.01%
primary salt flow rate Γ_1	[-]	-	1.14%	-	1.15%
intermediate salt flow rate Γ_2	[-]	-	1.20%	-	1.33%
ΔT primary salt	[K]	97.8	187.8	98.0	170.7
ΔT avg core	[K]	-	37.5	-	22.9
ΔT intermediate salt	[K]	84.77	151.9	79.1	119.7
ΔT water	[K]	113.9	252.2	107.2	121.5

2.5   Discussion and conclusions

The model presented in this chapter allows to simulate the thermal hydraulic behavior of a simplified design of the primary and intermediate circuit of the MSFR. Steady state and accidental condition were simulated with thermal hydraulic code TRACE. An available neutronic model for the transport of delayed neutron precursors was implemented in the code. This tool allowed to model the power variation during transients, coupling neutronics and thermal hydraulics. Moreover it allowed to simulate the decay heat distributed in the primary circuit.

The preliminary design of a printed circuit heat exchanger obtained in the previous chapter was successfully modeled with TRACE. The results for steady state operation agreed well (within 5%) with the expected results, providing a first code verification of the developed model.

The behavior of the system (in particular the primary heat exchanger) was studied for a station black out accident, where the primary and intermediate pump were tripped and no SCRAM was performed. Different configurations for the primary and intermediate circuit as well as the balance of plant were tested.

The strengthening of the natural circulation in the primary circuit was analyzed by increasing (to 4 m) the vertical distance between the core and the primary heat exchanger. The temperature difference (inlet-outlet) of the primary salt decreased after the transient, with respect to the nominal height difference (to 1.3 m). A lower temperature excursion improves the safety of the system, since freezing and boiling of the primary salt can be more easily prevented. This improvement required an increased primary salt volume (for the inlet and outlet pipes), nevertheless the constraints on the primary salt volumes follow several years of neutronic studies. Changes of this type in the design of the reactor should be therefore carefully investigated.

The effects of natural circulation in the intermediate circuit were tested by doubling the height difference between the primary and intermediate heat exchanger. A higher flow rate in the intermediate salt decreased slightly the power produced. The temperature difference between the hot and cold leg of the primary and intermediate circuit decreased as well, improving the safety of the system for this type of accident. A higher intermediate salt volume increases the thermal capacity of the intermediate circuit, which is in general favorable in case of accidents. A larger salt volume implies higher costs, which have not been analyzed in this work.

The balance of plant was modeled with a simple circuit with supercritical water, where the inlet temperature, pressure and flow rate are fixed in the intermediate heat exchanger. Different flow rates at the end of the transient were investigated. A too high flow rate causes an overcooling of the intermediate system, which increases the power production in the primary circuit and a higher maximal temperature of the primary salt, with respect to a lower water flow rate. In case of an unprotected loss-of-flow accident in the primary circuit, the manual decrease in flow rates in the intermediate circuit and balance of plant improves the safety of the system by reducing the power production.

Two different intermediate salts were investigated: FliBe and FliNaK. The configuration with FliNaK as intermediate salt exhibits a better performance in case of SBO accident through enhanced natural circulation, due to a larger thermal expansion coefficient. In the configuration with FliNaK the temperature difference (hot leg – cold leg) decreases for both primary and intermediate circuit, which is positive for safety. Moreover a slightly lower power is produced in the core.

The behavior of the system depending on height difference for core – primary HX and primary HX – intermediate HX, final water flow rates and different intermediate salt can be summarized as follows in terms of Γc_p ratio (r_i). This parameter was defined as the ratio between $\Gamma_i c_{p,i}$ for two fluids in a heat exchanger ($i = 1, 2$ representing the primary and intermediate HX), and describes the ratio between the "thermal inertia" of two flows. A large ratio r_2 (obtained by improving the natural circulation of the salt in

the intermediate circuit, and/or decreasing the water flow rate) seems to be favorable in case of a SBO accident (decrease in produced power and in maximal temperature of the primary salt). A large ratio $r_1 > 1$ is also favorable, since the temperature difference (between hot and cold leg) is reduced in the primary circuit with respect to the cases with $r_1 < 1$, while the temperature difference between hot and cold leg in the intermediate circuit remains constant.

Conclusions

Main results

The main goal of this thesis work was to develop a preliminary design of the primary heat exchanger (HX) for the Molten Salt Fast Reactor (MSFR) and to investigate the impact of the design on the reactor safety.

The main achievements of this work are here summarized:

- An assessment of currently available heat exchangers was performed for possible applications to the MSFR. A preliminary choice was conducted by comparing technological limits and design characteristics of HXs with the characteristics of the MSFR. Shell and tube heat exchanger (STHE) and printed circuit heat exchanger (PCHE) were selected as suitable types for further investigation. The STHE is the reference heat exchanger in the frame of power generation, while the PCHE is a relatively new and promising technology in the frame of compact heat exchangers.

- A software tool was developed with MATLAB for the preliminary design of both types of heat exchangers. The tool was applied to the constraints of the MSFR design considering power, inlet and outlet temperatures of the primary salt, pressure drops and salt volume. No configuration for the design of a STHE could be found given the constraints. Several possible configurations were found for a PCHE, featuring a high degree of compactness (121 MW/m^3), high intermediate salt outlet temperature (943 K) and relatively low pressure drops (4 bar) given the constraints of the MSFR. A trade-off design between smallest pressure drop and salt volume was selected for further investigations.

- The PCHE was modeled with the thermal hydraulic code TRACE in steady state conditions. Results obtained with TRACE for flow parameters and heat transfer coefficients showed good agreement (5% of discrepancy) with the predicted values from the MATLAB model.

- The capability of the MSFR to withstand an unprotected station black out (SBO) using the primary heat exchanger was tested. The primary and intermediate circuit together with a simple circuit for the power cycle were modeled using TRACE. The primary circuit was modeled with a core where the fluids heats up, a pump, the heat exchanger and the respective piping. The intermediate circuit was designed similarly, with the primary heat exchanger acting as heat source and a intermediate heat exchanger acting as heat sink. The power delivered to the salt in the primary circuit is controlled by a point neutron kinetics / 1-D precursors transport model.

  Effects of natural circulation (NC) on heat removal as well as temperature evolution in the designed system were investigated. Different configurations for the vertical displacement in the primary circuit (core – primary HX) and secondary circuit (primary HX – secondary HX) were tested. The following main conclusions can be drawn:

  - A stronger natural circulation in the primary circuit (obtained through a threefold vertical displacement between hot and cold well) decreases the maximal temperature reached by the primary salt (30%). The core average temperature increase between initial and final steady state is determined by the neutronics, and amounts to approximately 30 K, depending on the primary salt flow rate. The intermediate salt temperatures are not significantly affected by the change in flow rate in the primary circuit (less than 1% increase). The power produced in the primary circuit increases slightly because heat removal from primary circuit is improved. The temperature difference between hot and cold leg in the primary circuit decreases, due to an almost constant produced power and a higher salt flow rate. Therefore the safety of the system is improved.

  - The NC in the intermediate circuit was improved by doubling the height difference between primary and intermediate HX. The flow rate in the intermediate circuit increases by 25%. A higher flow rate in the intermediate circuit increases the thermal capacity of the salt flow (Γc_p), therefore the temperature difference between the hot and cold leg of the intermediate circuit decreases, for the same exchanged power. Furthermore, the temperature of the intermediate salt at the outlet of the intermediate heat exchanger is higher for the case where natural circulation is improved in the intermediate circuit, again due to a higher flow thermal capacity of the intermediate salt with respect to water. As a consequence, the temperature difference ΔT_{LM} between primary and intermediate salt in the primary heat exchanger decreases with respect to a lower intermediate salt flow rate. This reduces the power exchanged between the salts, which determines (through the heat balance in the system)

a decrease of the produced power. The maximal temperature in the primary circuit is finally reduced, which is positive from a safety point of view.

– The water flow rate at the end of the transient influences the behavior of the system. A high water flow rate decreases the intermediate salt temperature at the outlet of the intermediate heat exchanger. A low intermediate salt inlet temperature in the primary heat exchanger decreases the primary salt temperature in the cold leg. As a consequence the core outlet temperature rises, since the average temperature of the primary circuit is fixed by the neutronics. Furthermore the flow rate in the primary circuit is increased through a larger difference in the salt density between hot and cold well (stronger natural circulation). A larger temperature decrement of the primary salt in the heat exchanger and a higher primary salt flow rate determine a higher power produced in the circuit. In fact the MSFR is a load follower reactor. In case of a SBO accident a minimal water flow rate must be granted in order to remove the decay heat produced in the primary circuit. The intermediate salt must be cooled enough in the intermediate circuit in order to set up a natural circulation, responsible for the stabilization of the temperatures in the primary and intermediate circuit.

• Two configurations of the system have been investigated for two different intermediate salts: FliBe and FliNaK. A stronger natural circulation was observed for the configuration with FliNaK, mainly due to a larger thermal expansion coefficient. The temperature difference between hot leg and cold leg decreases for both primary and intermediate circuit, which is desirable from a safety point of view.

Future work to be considered

In this thesis work a preliminary design of the primary heat exchanger of the MSFR was investigated. An optimized design would require further studies on different branches. The following fields emerged as particularly relevant.

The primary heat exchanger was designed based on the constraints derived from studies on neutronics and core thermal hydraulics. These constraints were not modified even if their impact on the safety of the system – in terms of pressure drop – and on the effectiveness of the heat exchanger – in terms of intermediate salt outlet temperature – is significant. An optimized design of the primary circuit would require a joint study on neutronics, core and out-of-core thermal hydraulics, as well as on thermal efficiency of the MSFR.

A detailed analysis on the power generating circuit would be important in order to optimize the design of the intermediate heat exchanger. As emerged from this thesis work the heat removal from the intermediate circuit has a strong impact on temperature evolution in the primary circuit, therefore on the safety of the system. Simulations with a closed power generation circuit would allow a better evaluation of the impact of the intermediate heat exchanger on the system.

In this thesis a simplified model of the primary circuit was presented. A detailed model of the primary circuit would allow a more accurate evaluation of the thermal hydraulics and therefore of the behavior of the system in accidental conditions.

For a better safety assessment, simulations of different accidental scenario (e.g. partial pump coast-down, loss of heat sink, loss of flow in the primary circuit) would be needed.

Bibliography

[1] G. F. Hewitt, G. L. Shires, T. R. Bott, *Process Heat Transfer*, CRC press, 1994

[2] J. P. Holman, *Heat Transfer*, McGraw-Hill Book Company, 6th Edition, 1986

[3] C. Fiorina, *The Molten Salt Fast Reactor as a Fast-Spectrum Candidate for Thorium Implementation*, Politecnico di Milano, Doctoral Program in Energy and Nuclear Science and Technology, March 2013

[4] H. Rouch et al. *Preliminary thermal-hydraulic core design of the Molten Salt Fast Reactor (MSFR)*, Annals of Nuclear Energy, February 2014

[5] B. Yamaji et al. *Thermal-hydraulic analyses and experimental modelling of MSFR*, Annals of Nuclear Energy, February 2014

[6] E. Merle-Lucotte et al. *Launching the Thorium Fuel Cycle with the Molten Salt Fast Reactor*, Proceedings of the ICAPP 2011, France, May 2011

[7] M. Aufiero, *A few comments on the MSFR safety and design optimization*, Interactive talk, EVOL Meeting, France 2013

[8] E. Merle-Lucotte et al. *Recommendations for a demonstrator of Molten Salt Fast Reactor*, Fast Reactor International Conference, France 2013

[9] M. Aufiero et al. *Calculating the effective delayed neutron fraction in the Molten Salt Fast Reactor: Analytical, deterministic and Monte Carlo approaches*, Annals of Nuclear Energy, March 2014

[10] L. Luzzi et al. *An approach for the modelling and the analysis of the MSR thermo-hydrodynamic behaviour*, Chemical Engineering Science, August 2010

[11] A. Cammi et al. *Dimensional effects in the modeling of MSR dynamics: Moving on from simplified schemes of analysis to multi-physics modeling approach*, Nuclear Engineering and Design, May 2012

[12] H. G. MacPherson, *The Molten Salt Reactor Adventure*, Nuclear Science and Engineering, 1985

[13] M. W. Rosenthal, *An account of Oak Ridge National Laboratory's Thirteen Nuclear Reactors*, August 2009

[14] C. H. Gabbard, *Reactor power measurements and heat transfer performance in the molten salt reactor experiment*, ORNL-TM-3002, May 1970

[15] General engineering and construction division, *Design study of a heat-exchange system for one MSBR concept*, Technical Report ORNL-TM-1545, 1967

[16] V. Ariu, *Modeling for the primary heat exchanger used in the molten salt reactor experiment*, Semester work, PSI, 2013

[17] D. E. Holcomb et al. *An analysis of testing requirements for fluoride salt-cooled high temperature reactor components*, ORNL-TM-297, November 2009

[18] O. Beneš and R.J.M. Konigs *Molten Salt Reactor Fuel and Coolant*, p.364, Elsevier Ltd. 2012

[19] M. S. Sohal et al. *Engineering Database of Liquid Salt Thermophysical and Thermochemical Properties*, p.2, Idaho National Laboratory, 2010

[20] Floyd et al. *A numerical investigation of the sCO2 recompression cycle off-design behavior, coupled to a sodium cooled fast reactor, for seasonal variation in the heat sink temperature*, Nuclear Engineering and Design, July 2013

[21] A. Moisseytsev, J. J. Sienicki, *Investigation of alternative layouts for the supercritical carbon dioxide Brayton cycle for a sodium-cooled fast reactor*, Nuclear Engineering and Design, March 2009

[22] V. Dostal et al. *The supercritical carbon dioxide power cycle: comparison to other advanced power cycles*, Nuclear Technology, June 2006

[23] V. Dostal, *A supercritical carbon dioxide cycle for next generation nuclear reactors*, MIT-ANP-TR-100, March 2004

[24] E. A. Harvego, M.G. McKellar, *Evaluation and optimization of a supercritical carbon dioxide power conversion cycle for nuclear applications*, Proceedings of the 19th International Conference on Nuclear Engineering, Japan, May 2011

[25] Su et al. *Optimization study for thermal efficiency of supercritical water reactor nuclear power plant*, Annals of Nuclear Energy, January 2014

[26] C. Boehm et al. *Supercritical steam cycle for lead cooled nuclear systems*, Proceedings of GLOBAL, Japan, October 2005

[27] M. Naidin et al. *Super critical water-cooled nuclear reactors (SCWRs) thermodynamic cycle options and thermal aspects of pressure-channel design*, IAEA-CN-164-5S03

[28] Mokry et al. *Thermal hydraulic analysis and heat transfer correlation for an intermediate heat exchanger linking a SuperCritical Water-cooled Reactor and a Copper-Chlorine cycle for hydrogen co-generation*, International Journal of Hydrogen Energy, November 2012

[29] F. Cziesla et al. *Lünen – State-of-the-art ultra supercritical steam power plant under construction*, POWER-GEN Europe 2009 - Cologne, Germany, May 2009

[30] *http://www.energy.siemens.com/co/pool/hq/power-generation/steam-turbines/downloads/steam-turbine-for-csp-plants-siemens.pdf*, Steam turbine for CSP plant

[31] A.A. Adams, *Design considerations of a 15 kW heat exchanger for the CSPonD Project* MIT, June 2010

[32] D. Kearney et al. *Assessment of a molten salt heat transfer fluid in a parabolic trough solar field* J. Sol. Energy Eng, May 2003

[33] M. A. Ravagnani et al. *Heat analysis and thermodynamic effects*, Chapter 7, Optimal shell and tube heat exchangers design, InTech, September 2011

[34] R. Mukherjee, *Effectively Design Shell-and-Tube Heat Exchangers*, Chemical Engineering Progress, 1998

[35] M. S. Peters, K. Timmerhaus, R. E. West, *Plant Design and Economics for Chemical Engineers*, Chapter 14: "Heat-Transfer Equipment – Design and Costs", McGraw-Hill Book Company, 2003

[36] R.W. Serth, *Process heat transfer: principles, applications and rules of thumb*, Academic Press, 2007

[37] K. Thulukkanam, *Heat Exchanger Design Handbook*, CRC Press, 2nd Edition, 2013

[38] D. Aquaro, M. Pieve, *High temperature heat exchangers for power plants: Performance of advanced metallic recuperators*, Applied Thermal Engineering, February 2007

[39] John E. Hesselgreaves, *Compact Heat Exchangers, Selection, Design and Operation*, Elsevier, 2001

[40] *http://www.heatric.com*, July 2014

[41] Figley et al. *Numerical study on the thermal hydraulic performance of a Printed Circuit Heat Exchanger*, Progress in Nuclear Energy, September 2013

[42] I. Kim, H. No, *Physical model development and optimal design of PCHE for intermediate heat exchangers in HTGRs*, Nuclear Engineering and Design, February 2012

[43] I. Kim et al. *Thermal hydraulic performance analysis of a printed circuit heat exchanger using a helium-water test loop and numerical simulations*, Nuclear Engineering and Design, November 2011

[44] I. Kim et al. *Thermal hydraulic performance analysis of the printed circuit heat exchanger using a helium test facility and CFD simulations*, Nuclear Engineering and Design, November 2009

[45] S. Yoon et al. *Numerical study on crossflow printed circuit heat exchanger for advanced small modular reactors*, International Journal of Heat and Mass Transfer, March 2014

[46] *www.haynesintl.com*, Properties of Hastelloy® N, July 2014

[47] *www.turbomachinerymag.com*, July 2014

[48] *http://www.offshoreenergytoday.com*, May 2014

[49] *http://www.emeraldinsight.com*, July 2014

[50] *www.eia.gov/forecast/ieo*, International Energy Outlook 2013, U.S. Energy Information Administration

[51] *www.world-nuclear.org/info/Nuclear-Fuel-Cycle/Power-Reactors*

[52] *http://www.world-nuclear.org/info/ Non-Power-Nuclear-Applications/Industry/ Nuclear-Process-Heat-for-Industry/*, Nuclear process heat for industry, July 2014

[53] *http://www.gen-4.org/Technology/systems/index.htm*

[54] *TRACE V5.0 User's Manual*, Volume 1, December 2011

Acronyms and abbreviations

ANP	Aircraft Nuclear Propulsion
ARE	Aircraft Reactor Experiment
CHE	Compact Heat Exchanger
CNRS	Centre National de la Recherche Scientifique
CSP	Concentrated Solar Power
DNP	Delayed Neutron Precursors
EVOL	Evaluation and Viability Of Liquid fuel fast reactor systems
HTC	Heat Transfer Coefficient
HX	Heat Exchanger
IAPWS	International Association for the Properties of Water and Steam
FliBe	LiF-BeF$_2$
FliNaK	LiF-NaF-KF
FP	Fission Products
STHE	Shell and Tube Heat Exchanger
PCHE	Printed Circuit Heat Exchanger
MSR	Molten Salt Reactor
MSBR	Molten Salt Breeding Reactor
MSFR	Molten Salt Fast Reactor
MSRE	Molten Salt Reactor Experiment
ORNL	Oak Ridge National Laboratory
PFHE	Plate Fin Heat Exchanger
PHE	Plate Heat Exchanger
POLIMI	Politecnico di Milano
PSI	Paul Scherrer Institute
RIA	Reactivity Induced Accident
SBO	Station Black Out
TEMA	Tubular Exchanger Manufacturers' Association
TRACE	TRAC/RELAP Advanced Computational Engine

Nomenclature

<u>Latin symbols</u>

A	Area	m^2
B_c	Baffle-cut	m
c_p	Heat capacity	J/kg·K
D_{ctl}	Centerline tube limit	m
D_h	Hydraulic diameter	m
D_s	Shell diameter	m
d	Diameter	m
d_i	Tube inner diameter	m
d_o	Tube outer diameter	m
F_c	Fraction of tubes in crossflow	-
f	Friction factor	-
k	Thermal conductivity	W/m·K
J_B	Bypass correction factor	-
J_c	Configuration correction factor	-
J_L	Leakage correction factor	-
L	Length	m
L_{tube}	Tube length	m
L_{tp}	Tube pitch	m
L_{bc}	Baffle spacing	m
L_{sb}	Shell-to-baffle diametral clearance	m
L_{bb}	Bundle-to-shell diametral clearance	m
L_{tb}	Tube-to-baffle diametral clearance	m
$\dot{M}$	Mass flux	kg/m^2·s
N	Number of baffles	-
Nu	Nusselt number	-
N_t	Number of tubes	-
N_p	Number of tube passes	-
P	Tube pitch	m
Pr	Prandtl number	-
$\dot{Q}$	Power	W
$\dot{q}''$	Heat flux	W/m^2
Re	Reynolds number	-
SS	Sealing strips per crossflow row	-
T	Temperature	K
ΔT_M	Average temperature	K
t_p	Plate thickness	m

t_w	Tube thickness	-
U	Heat transfer coefficient	W/m^2·K
$\tilde{U}$	Non-dimensional heat transfer coefficient	-
V	Volume	m^3
$\dot{V}$	Volumetric flow rate	m^3/s
v	Velocity	m/s
$\tilde{x}$	Non-dimensional length	-

Greek symbols

α	Feedback coefficient	-/s
Δp	Pressure drop	bar
ΔT_M	Average temperature difference	K
ΔT_{LM}	Logarithmic mean temperature difference	K
Γ	Mass flow rate	kg/s
λ	Decay constant	1/s
μ	Dynamic viscosity	Pa·s
∇	Gradient	1/m
ρ	Density	kg/m^3
θ	Non-dimensional temperature	-

Acknowledgements

There are many people I would like to thank for their priceless help and support throughout my studies and in particular this master thesis.

I would like to thank my tutor Prof. Michael Prasser. His wide expertise in nuclear engineering is a constant source of motivation for me. I wish to thank Prof. Andreas Pautz for his precious guidance during these two years of the master program. I would like to express my deep gratitude to my supervisor Dr. Carlo Fiorina for his invaluable support during my master thesis. I am really grateful to my supervisor Dr. Konstantin Mikityuk for his patient help with TRACE and his precious guidance throughout this research work. Thanks to Matteo Zanetti for his help with the dnp solver. I would like to thank Sara, Boris, Ann-Lo and Miquel, for sharing the same office at PSI for six month, and all the people in the FAST group for setting up this friendly and collaborative environment.

Let's move to Ticino and continue in Italian. Ci tengo a ringraziare le montagne della Val Bedretto per avermi regalato attimi di tregua dallo studio e per avermi permesso di ricaricare le batterie quando necessario. Ringrazio i miei amici e compagni di cordata Stellino, Luca, Jacky, Bene, Linda e Jordy che mi hanno sostenuto, sia in montagna sia nello studio. Grazie anche a Frigi, Monica, Nick, Nick (l'altro) e Sofy, amici che mi hanno incoraggiato a studiare anche durante le lunghe estati in cui scomparivo in una biblioteca di Zurigo.

Vorrei ringraziare i miei genitori Manuela e Giuseppe e mia sorella Astrid, per avermi motivato quando ne avevo bisogno e supportato in ogni modo (e sopportato negli ultimi tempi!). Solo grazie a loro è stato possibile questo percorso.